JOURNAL OF PETROLOGY | VOLUME 40 | NUMBER 4 | PAGES 629–652 | 1999

The Stability of Hydrous Potassic Phases in Lherzolitic Mantle—an Experimental Study to 9·5 GPa in Simplified and Natural Bulk Compositions

J. KONZETT* AND P. ULMER

INSTITUT FÜR MINERALOGIE UND PETROGRAPHIE, ETH-ZENTRUM, SONNEGGSTR. 5, CH-8092 ZÜRICH, SWITZERLAND

RECEIVED JANUARY 30, 1998; REVISED TYPESCRIPT ACCEPTED SEPTEMBER 30, 1998

To investigate the pressure stability limit of phlogopite and the pressure–temperature stability field of its breakdown product K-richterite, experiments were conducted from 4·0 to 9·5 GPa and between 800°C and 1400°C in a subalkaline system K_2O–Na_2O–CaO–MgO–Al_2O_3–SiO_2–H_2O (KNCMASH) and in natural phlogopite and K-richterite-doped lherzolite systems. In KNCMASH, phlogopite breaks down between 6·0 and 6·5 GPa at 800°C and between 6·5 and 7·0 GPa at 1100°C to form potassic amphibole by the reaction phlogopite + clinopyroxene + orthopyroxene = K-richterite + garnet + olivine + H_2O. In the natural system, the stability field of amphibole is shifted towards lower pressures by ~0·5 GPa. The high-temperature stability limit of K-richterite in KNCMASH was located between 1300 and 1400°C at 8·0 GPa and at <1300°C at 7·0 GPa. Thus, K-richterite can be stable in the mantle wedge above subduction zones below a depth of ~180–200 km. Because of the small difference in K/OH ratios between phlogopite and K-richterite, only a small amount of aqueous fluid is likely to be produced during phlogopite breakdown in an average mantle lherzolite bulk composition. This fluid might be trapped by nominally anhydrous minerals before it can migrate to hotter portions of the mantle wedge. Phlogopite breakdown therefore is unlikely to be a factor in inducing significant melting of the wedge leading to arc magmatism.

KEY WORDS: *experimental study; high pressure; K-richterite; lherzolite; phlogopite*

INTRODUCTION

Hydrous potassic phases are potential hosts for alkalis and H_2O in metasomatized lherzolitic mantle to depths near the transition zone (Trønnes *et al.*, 1988; Trønnes, 1990) and are likely to be source components for deep-seated generation of potassium-rich magmas (e.g. Wendlandt & Eggler, 1980; Lloyd *et al.*, 1985; Foley, 1992; Thibault *et al.*, 1992; Mitchell, 1995; Luhr, 1997). The hydrous phases phlogopite and K-rich richteritic amphibole are potentially stable in natural peridotitic bulk compositions and carry significant amounts of potassium and water. Phlogopite–spinel peridotites are common in xenolith suites of metasomatized shallow upper mantle sampled by basaltic volcanism (Nixon, 1987, and references therein), whereas phlogopite–garnet peridotites are typically part of xenolith suites from deep continental lithosphere. In rare cases K-richterite-bearing peridotites are found as xenoliths in kimberlites (e.g. Erlank *et al.*, 1987; Tallarico & Leonardos, 1995). Although phlogopite peridotites typically show well-equilibrated textures, textures of K-richterite-bearing peridotites indicate that the amphibole is not in equilibrium with the host lherzolite (Erlank *et al.*, 1987). The occurrence of diamond-bearing phlogopite peridotites (Dawson & Smith, 1975; Waters & Erlank, 1988) testifies that phlogopite is stable above 4 GPa in peridotitic bulk compositions under cool lithospheric P–T conditions. With respect to T, phlogopite is stable in lherzolite to <1250°C at 3·0 GPa under water-absent conditions and to <1150°C at the same pressure

*Corresponding author. Present address: Geophysical Laboratory, 5251 Broad Branch Road, N.W., Washington, DC 20015-1305, USA. Telephone: 202-686-2410, ext. 2443. Fax: 202-686-2419.
e-mail: konzett@gl.ciw.edu

Table 1: Composition of synthetic and natural starting materials used in this study compared with starting materials of previous experimental studies and of natural metasomatized peridotites from the Kaapvaal Craton

	KNCMASH bulk	Modified BRIAN 2 + phl	Modified BRIAN 2 + Kr	Kr synth (n = 10)	KE70	T88	ST90, L97	BRIAN 2	KLB-1	Average sp lherz	Average PKP
SiO_2	47·28	45·35	46·56	57·22(20)	48·96	43·78	49·35	44·13(37)	44·48	44·20	42·72
TiO_2	—	0·12	0·12	—	2·35	0·11	—	0·09(03)	0·16	0·13	0·06
Al_2O_3	11·50	4·37	3·60	—	9·20	6·42	6·10	2·76(07)	3·59	2·05	1·31
Cr_2O_3	—	0·69	0·66	—	—	0·21	—	0·49(04)	0·31	0·44	0·41
FeO*	—	6·95	6·66	—	—	—	—	7·92(18)	8·10	8·29	—
Fe_2O_3	—	—	—	—	2·16	5·96	—	—	—	—	7·09
MnO	—	0·08	0·07	—	0·04	0·08	—	0·08(04)	0·12	0·13	0·12
MgO	27·26	37·24	36·47	24·20(22)	20·59	35·59	23·80	41·32(14)	39·22	42·21	41·33
CaO	6·58	3·55	4·00	6·71(19)	9·07	2·28	12·96	2·63(09)	3·44	1·92	1·33
Na_2O	1·22	0·69	1·08	4·61(09)	2·42	0·20	—	0·22(03)	0·30	0·27	0·16
K_2O	4·94	0·54	0·38	4·16(11)	3·79	3·75	5·64	<0·05	0·02	0·06	0·16
P_2O_5	—	n.d.	—	—	—	0·02	—	n.d.	0·03	0·03	0·05
NiO	—	0·21	0·20	—	—	0·17	—	0·27(07)	0·25	0·28	0·27
LOI	—	—	—	—	—	—	—	—	—	—	4·66
H_2O	1·22	0·21	0·20	2·15(01)	1·42	1·43	2·15	—	—	—	—
Σ	100·00	100·00	100·00	99·05(61)	100·00	100·00	100·00	99·93(53)	100·02	100·01	99·49
wt % ol								63·3	58·0	66·7	
wt % opx								22·5	25·0	23·7	
wt % cpx								11·9	15·0	7·8	
wt % sp								2·3	2·0	1·7	
PI	0·64	0·39	0·61	—	0·88	0·68	1·00	0·13	0·14	0·25	0·34
K/Na	2·66	0·51	0·23	0·59	1·03	12·33	—	≤0·14	0·04	0·15	0·65

ST90, L97, Sudo & Tatsumi (1990) and Luth (1997), even-weight mixture of pure synthetic phlogopite + diopside; KE70, Kushiro & Erlank (1970), 2:1 mixture of synthetic pyrope$_2$grossular$_1$ + natural K-richterite, K-richterite composition taken from Prider (1939); T88, Trønnes *et al.* (1988) calculated as mix of 66 wt % peridotite KLB-1 (Takahashi, 1986) + 33 wt % pure phlogopite (see Luth *et al.*, 1993); BRIAN 2, average of 10 glass analyses of spinel lherzolite BRIAN 2; modified BRIAN 2 + phl, BRIAN 2 after addition of 5 wt % synthetic phlogopite (phlogopite composition assumed to be stoichiometric), 0·4 wt % Na_2O, and after subtraction of 30 wt % olivine (Fo_{91}); modified BRIAN 2 + Kr, BRIAN 2 after addition of 10 wt % synthetic K-richterite (Kr synth), 0·4 wt % Na_2O, and after subtraction of 30 wt % olivine (Fo_{91}); PKP, average of 24 bulk analyses of garnet–phlogopite peridotites (GPPs) given by Erlank *et al.* (1987); average sp lherz, average of 384 analyses of spinel lherzolite xenoliths (Maaløe & Aoki, 1977); PI (peralkalinity index) = molar $(K_2O + Na_2O)/Al_2O_3$.
*Fe_{tot} given as FeO.

under water-saturated conditions (Wendlandt & Eggler, 1980), consistent with results of Mengel & Green (1989).

Experimental work in the KCMASH system has shown that phlogopite + clinopyroxene ± orthopyroxene assemblages break down to form KK-richterite[1] + garnet + olivine at $P \geq 6$–7 GPa or ~180–210 km, thus making phlogopite-bearing peridotites potential host rocks for potassium amphibole (Sudo & Tatsumi, 1990; Luth, 1997). This suggests that in a subalkaline[2] bulk composition K-amphibole can be stable in mantle regions only where K–OH metasomatism is active within the diamond stability field or where metasomatized phlogopite-bearing mantle can be transported to a depth exceeding the upper-pressure stability limit of phlogopite. At present, no K-richterite-bearing peridotites have been found in which the amphibole is in textural equilibrium

[1]Throughout this study, the terms 'KK-richterite' and 'K-richterite' will be used to refer to amphiboles with the idealized composition $KKCaMg_5Si_8O_{22}(OH)_2$ and $KNaCaMg_5Si_8O_{22}(OH)_2$, respectively.

[2]Throughout this study, the term subalkaline will be used to refer to bulk compositions with molar $(K_2O + Na_2O)/Al_2O_3$ <1·0 as opposed to peralkaline compositions with molar $(K_2O + Na_2O)/Al_2O_3$ >1·0.

Table 2: Summary of experimental run conditions and run products

Exp. no.	Capsule material	*P* (GPa)	*T* (°C) TC_1	*T* (°C) TC_2	*T* (°C) Ca in opx	Run time	Phases detected
Ma60s*	Pt	4·0	1100	—	1102±12	16h11	phl + cpx + opx + ga
Ma62s	Pt	8·0	1100	—		20h49	phl + cpx + ga + Kr + ol
Ma63s	Pt	6·0	1100	—	1106±37	24h43	phl + cpx + opx + ga
Ma64s	Pt	7·0	1100	—		30h27	phl + cpx + ga + Kr + ol
Ma76s	Pt	6·5	800	—		74h08	phl + cpx + ga + Kr + ol
Ma80s	Pt	6·0	800	783		96h31	phl + cpx† + ga + ol
Ma81s	Pt	6·5	1100	1087	1118±28	24h21	phl + cpx + opx + ga + ol
Ma83s	Pt	6·5	950	—	966±27	50h46	phl + cpx + opx + ga + ol + Q
Ma85s	Pt	5·0	1100	—	1092±24	27h48	phl + cpx + opx + ga
Ma86s	Pt	6·5	850	—		96h13	phl + cpx + ga + Kr + ol
Ma96s	Pt	8·0	1300	1317		02h06	cpx + ga + Kr + ol + opx
Ma99s	Pt	9·0	1100	—		06h45	cpx + ga + Kr + ol + Q
Ma100s	Pt	8·0	1400	—		02h08	cpx + ga + ol + opx + Q
Ma101s	Pt	7·0	1300	—		14h53	cpx + ga + ol + opx + Q
Ma106s	Pt	8·0	1200	—		24h48	cpx + ga + ol + opx + Q
PU620*	Pt	7·0	1100	—		24h40	cpx + ga + ol + opx + Kr
PU624	Pt	6·0	1100	—		29h06	cpx + ga + ol + opx + phl
PU633	Pt	6·5	1100	—		32h00	cpx + ga + ol + opx + Kr + phl
PU638	Pt + C	6·5	1100	—	1101±17	49h54	cpx + ga + ol + opx + Kr
PU643	Pt + C	8·0	1100	—		99h00	cpx + ga + ol + opx + Kr
PU644	Pt + C	8·0	1300	—		42h36	cpx + ga + ol + opx
PU647	Pt + C	8·0	1400	—		03h12	cpx + ga + ol + opx
PU649	Pt + C	8·0	1200	—		51h36	cpx + ga + ol + opx + Kr
PU654	Pt + C	6·0	1100	—		42h00	cpx + ga + ol + opx + phl
PU667‡	Pt + C	9·5	1200	—		27h20	cpx + ga + ol + opx
PU698‡	Pt + C	9·5	1300	—		17h40	cpx + ga + ol + opx

Abbreviations are given in Table 9.
*Ma run numbers refer to runs in the simplified KNCMASH system; PU numbers refer to runs in the natural peridotite system doped with phl or Kr.
†Two coexisting clinopyroxenes.
‡Runs doped with 10% Kr; TC_1 thermocouple at capsule bottom; TC_2 thermocouple attached to capsule wall (see Konzett *et al.*, 1997).

with the lherzolitic host assemblage. Nevertheless, the widespread occurrence of K-richterite in equilibrium with a garnet lherzolite assemblage in subduction zone peridotites has been proposed by Tatsumi (1989), Tatsumi *et al.* (1991) and Tatsumi & Eggins (1995), on the basis of the stability of phlogopite in the peridotitic mantle wedge above subducting slabs and experimental results of Sudo & Tatsumi (1990). Tatsumi & Eggins (1995) proposed that fluids released by the phlogopite-to-potassium amphibole reaction can trigger the mantle melting responsible for arc volcanism above subduction zones. Only reconnaissance studies have been available to date on the stability field of K-richterite in subalkaline bulk compositions relevant to normal lherzolitic mantle compositions (Trønnes *et al.*, 1988; Trønnes, 1990; Harlow, 1995). The principal objectives of this study therefore were to locate the *P*–*T* conditions of the reaction by which phlogopite breaks down to form amphibole precisely and determine the phase compositions across the phlogopite–amphibole transition so as to assess the amount of fluid released during phlogopite breakdown. The KNCMASH system was studied first to avoid the complications arising from heterovalent cation substitutions and bulk compositional change from reaction of the experimental

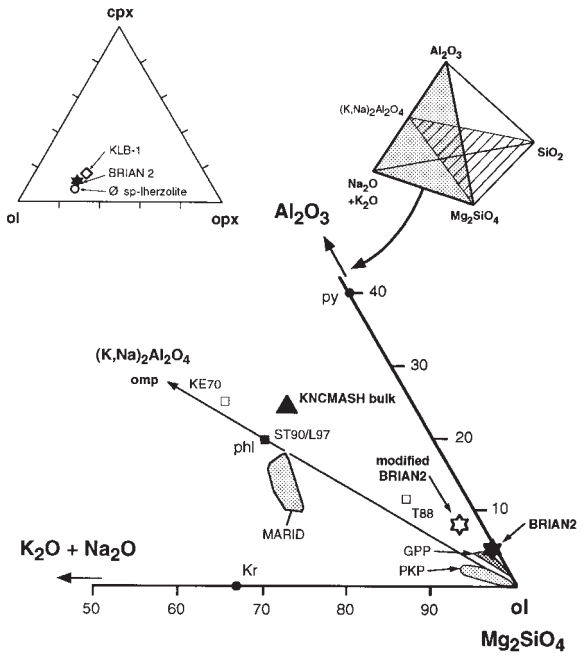

Fig. 1. Projection from the SiO_2 apex onto the Al_2O_3–(Na_2O + K_2O)–Mg_2SiO_4 plane of the KNMAS tetrahedron (Sweeney *et al.*, 1993) (inset upper right). ▲, simplified KNCMASH bulk composition; ★, spinel lherzolite BRIAN 2; ☆: modified BRIAN 2 (30 wt % olivine subtracted, 0·4 wt % Na_2O and 5 wt % phlogopite added). ●, compositions of pure K-richterite, phlogopite and pyrope. □, bulk compositions used by Kushiro & Erlank (1970) (KE70), Sudo & Tatsumi (1990) (ST90), Luth (1997) (L97) and Trønnes *et al.* (1988) (T88). Shaded areas: compositional range of MARID (mica–amphibole–rutile–ilmenite–phlogopite) xenoliths (Waters, 1987*a*), PKP (phlogopite–K-richterite–peridotite) and GPP (garnet–phlogopite–peridotite) xenoliths (Erlank *et al.*, 1987). The inset upper left triangle shows the modal composition of BRIAN 2 in wt % of olivine, orthopyroxene and clinopyroxene compared with the composition of average spinel lherzolite (Maaløe & Aoki, 1977) and of fertile spinel lherzolite KLB-1 (Takahashi, 1986). (For abbreviations, see Table 9, below.)

charge with the noble metal capsule. In a second step, experiments were performed using a natural lherzolite composition doped with phlogopite or K-richterite.

PREVIOUS EXPERIMENTAL WORK

Kushiro & Erlank (1970) first reported K-richterite breakdown to phlogopite in the presence of garnet at 1000°C at 2·0 GPa and proposed a reaction

$$\text{K-richterite} + \text{garnet}_{ss} = \text{phlogopite} + \text{clinopyroxene}_{ss} + \text{orthopyroxene} \quad (1)$$

$$KNaCaMg_5Si_8O_{22}(OH)_2 + CaMg_2Al_2Si_3O_{12} = KMg_3AlSi_3O_{10}(OH)_2 + 2\ CaMgSi_2O_6{\cdot}NaAlSi_2O_6 + 2\ MgSiO_3. \quad (1a)$$

This reaction accounts for the *P*-induced breakdown of phlogopite in lherzolites or websterites into which phlogopite was introduced by metasomatic melts or fluids. Subsequent experimental studies on the stability of pure K-richterite (Trønnes, 1990; Foley, 1991) constrained the maximum stability field of amphibole and thus are of restricted relevance to real mantle rocks. Sudo & Tatsumi (1990) and Luth (1997) investigated the stability field of KK-richterite in a KCMASH system using phlogopite + diopside or phlogopite + diopside + enstatite mixes as starting materials. Sudo & Tatsumi (1990) proposed that a reaction of the form

$$\text{phlogopite} + \text{diopside} \pm \text{enstatite} = \text{K-amphibole} + \text{garnet} + \text{olivine} + \text{fluid} \quad (2)$$

governs the stability of phlogopite in the upper mantle. Harlow (1995) used an Na-free system to investigate the influence of halogens on K-amphibole stability to 11 GPa. Thibault (1993) used phlogopite + diopside mixes in a KNCMASH(F) system. This system considers jadeite–diopside and K-richterite–richterite solid solution but rules out orthopyroxene as a potential reactant for the formation of amphibole.

COMPOSITION AND PREPARATION OF THE STARTING MATERIAL

Our starting composition in the KNCMASH system contains an excess of phlogopite relative to orthopyroxene and thus can be used to locate the upper-pressure stability limit of phlogopite in the presence of K-richterite (Table 1, Fig. 1). A spinel lherzolite from Mont Briançon, French Massif Central, was used as natural starting material (see Downes, 1987) because it represents a moderately fertile bulk composition slightly higher in modal clinopyroxene than average spinel lherzolite but less fertile than KLB-1 (see Table 1, Fig. 1). This composition was modified by subtracting 30 wt % olivine (Fo_{91}) to increase the amount of pyroxenes relative to olivine and by adding 5 wt % synthetic phlogopite and 0·4 wt % Na_2O. For two runs within the K-richterite stability field (PU667, PU698; see Table 2) the lherzolite was doped with 10 wt % synthetic K-richterite. Phlogopite and K-richterite were used as carriers for both potassium and water, with 5 and 10 wt % representing a minimum amount that contains sufficient potassium to produce detectable quantities of potassic phases in the experiments. Although in the natural system an excess of orthopyroxene with respect to phlogopite is present, phlogopite could still 'survive' the amphibole formation and coexist with K-richterite as a result of exhaustion of jadeite component in clinopyroxene. To avoid this less realistic scenario, 0·4 wt % Na_2O was added to the natural starting material.

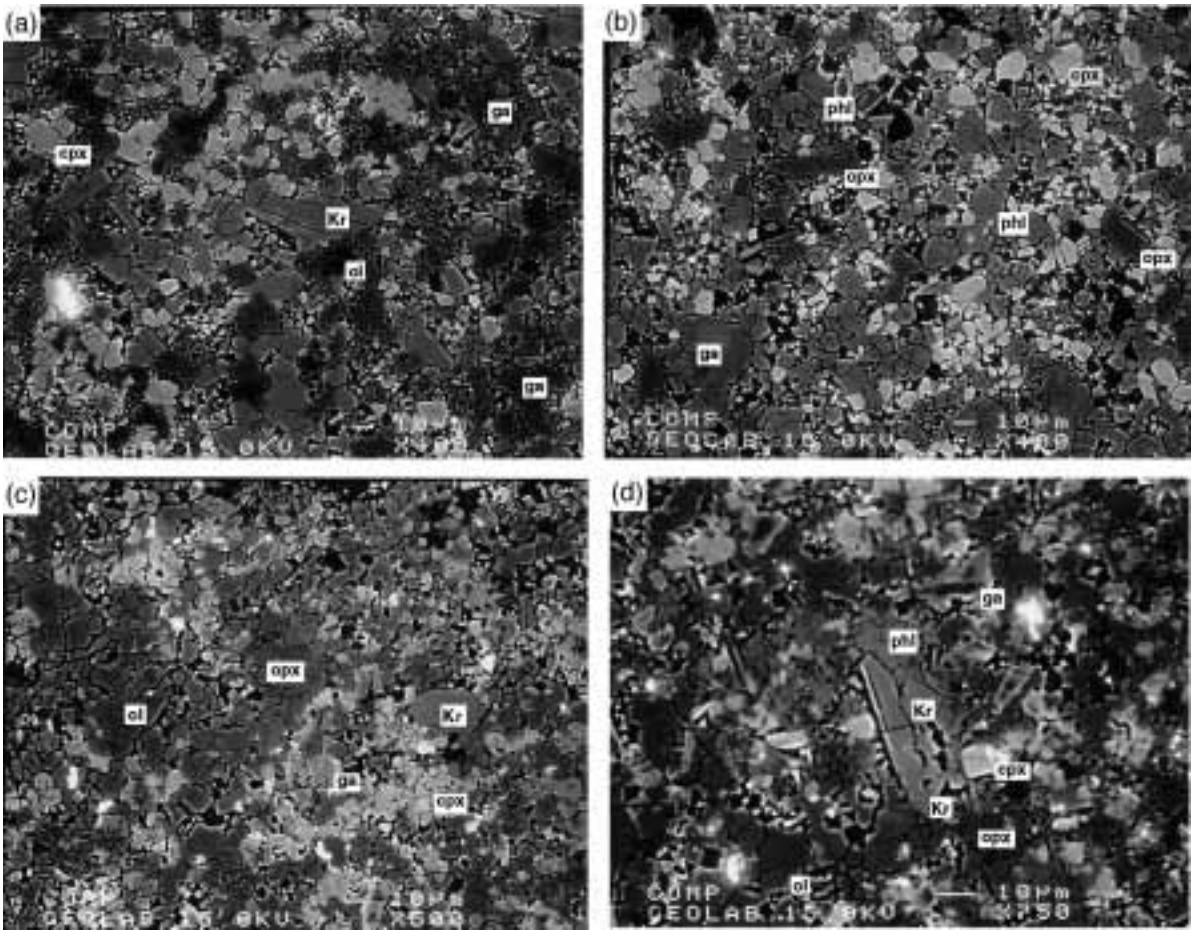

Fig. 2. Back-scattered electron photomicrographs of experimental charges from simplified and natural bulk compositions. (a) Ma62s (8 GPa, 1100°C), KNCMASH above the K-richterite-in reaction; (b) Ma85s (5 GPa, 1100°C), KNCMASH below the K-richterite-in reaction; (c) PU649 (8 GPa, 1200°C), Pt_{100} + inner graphite capsule; (d) PU633 (6·5 GPa, 1100°C), Pt_{100} capsule with coexisting K-richterite + phlogopite. (For abbreviations, see Table 9, below.)

Preparation of the starting materials

For the simplified KNCMASH bulk composition, a mix of synthetic oxides and carbonates was used. H_2O was added to the anhydrous oxide mix as $Mg(OH)_2$ and Na_2O as sodium metasilicate (Na_2SiO_3). Details of the preparation procedure have been given by Konzett *et al.* (1997). The natural starting composition (modified BRIAN 2) used synthetic oxides and carbonates, with FeO added as synthetic fayalite and Na_2O as sodium metasilicate. Phlogopite and K-richterite were synthesized at 0·3 GPa and 680°C, and 3·0 GPa and 1000°C, respectively, from oxide–carbonate mixes. Phlogopite turned out to be too fine grained for reliable microprobe analysis; X-ray diffraction showed the presence of well-crystallized phlogopite without additional diffraction lines. K-richterite was large enough (up to 15 μm) to be analysed with the electron microprobe; an averaged composition is given in Table 1. After mixing, the starting materials were stored at 250°C to minimize adsorption of moisture.

EXPERIMENTAL AND ANALYTICAL TECHNIQUES

Experiments were performed in a Walker-type two-stage 6/8 multi-anvil module (Walker *et al.*, 1990; Walker, 1991) in a 1000 ton press. The pressure-transmitting octahedra and gasket fins are fabricated from an MgO-based castable ceramic. For runs to 9·5 GPa (including the high-temperature calibration runs), 3·5 mm outer diameter (o.d.) stepped graphite furnace assemblies, in combination with WC cubes with a truncated edge length (TEL) of 12 mm were used. The run at 9·0 GPa (Ma99s) was conducted with 8 mm TEL WC cubes and a 3·5 mm $LaCrO_3$ stepped heater assembly. Temperatures were

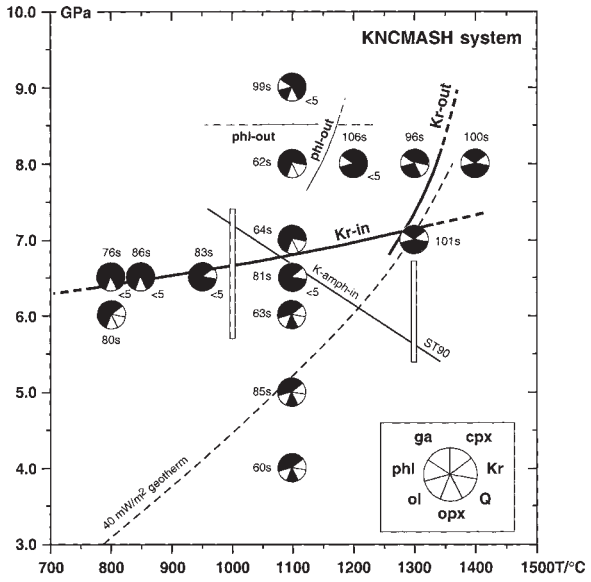

Fig. 3. *P–T* diagram of experimental results in the KNCMASH system (Table 1). Phases present in the experimental charges are represented by black sectors within the run symbol; phases not detected are denoted by white sectors (inset lower right). The dashed line is a 40 mW/m^2 continental geotherm (Pollack & Chapman, 1977). The numbers next to the run symbols are run numbers (Table 2) and observed approximate amounts of quench products. Vertical bars denote the *P* range within which Sudo & Tatsumi (1990) located the K-amphibole-in-reaction (ST90) (see their fig. 1).

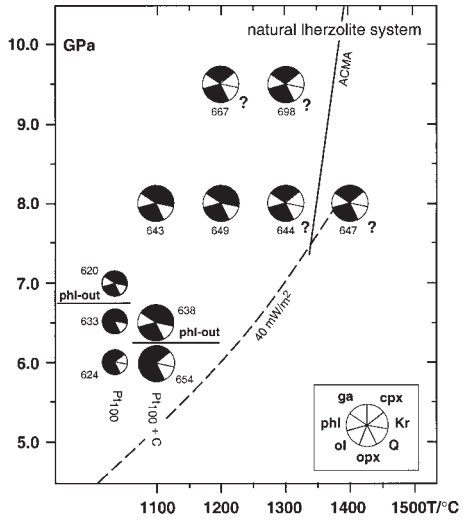

Fig. 4. *P–T* diagram summarizing experimental results using a natural lherzolite starting composition (Table 1). Symbols and 40 mW/m^2 geotherm are as in Fig. 3. ACMA is an average current mantle adiabat for a surface potential temperature of 1280°C (Thompson, 1992). Numbers next to run symbols are run numbers (Table 2). All runs except PU667 and PU698 had 5 wt % phlogopite added; PU667 and PU698 had 10 wt % K-richterite added.

measured with one thermocouple at the bottom of the capsule and in some experiments with a second thermocouple attached to the capsule wall (see fig. 2 of Konzett *et al.*, 1997). Temperature gradients measured with this arrangement do not exceed 30°C/mm; the vertical length of the experimental charge is $\leq 1{\cdot}5$ mm. All temperatures quoted are thermocouple readings from the Eurotherm controller uncorrected for the pressure effect on e.m.f. During the runs temperatures were kept constant to within ± 2°C and the applied load to within ± 1 ton (strain-gauge reading; corresponding to $\leq 0{\cdot}02$ GPa) and recorded during the entire duration of the experiment. Details of the calibration procedure have been given by Konzett *et al.* (1997). For runs in the simplified KNCMASH system, 1·6 mm o.d. Pt_{100} capsules were used. Except for three runs (Table 2), experiments using the lherzolite starting composition were conducted in 1·6 mm o.d. Pt_{100} capsules, with an inner graphite capsule to reduce $f(O_2)$ within the experimental charge relative to $f(O_2)$ in Pt_{100} capsules and to avoid loss of Fe to the capsule wall.

Analytical technique

After each experiment, capsules were embedded longitudinally in epoxy resin and ground to expose the centre of the charge. During opening of the KNCMASH charges small amounts of water extruded from the capsules, which was taken as an indication of water-saturated conditions at subsolidus temperatures and of integrity of the capsule during the run. Run products were analysed with a Cameca SX50 electron microprobe at ETH Zürich and with a JEOL Superprobe at the Geophysical Laboratory. The following standards were used: Si, Ti, Cr, Al, Mg: synthetic oxides; Ca, Fe, Mn, Na, K: natural wollastonite, haematite, tephroite, aegirine or omphacite, and orthoclase. Correction of the raw data was performed on-line with the PAP (ETH) or the PRZ (Geophysical Laboratory) correction procedure. Analytical conditions were 15 kV acceleration voltage and 20 nA sample current; the beam size was minimized (~1 μm) for most analyses, except for analyses of phlogopite and amphibole if the grain size was sufficiently large. Counting times of 20 s on peaks and 10 s on backgrounds were used. Ni in the experimental charges was analysed using synthetic NiO as a standard and counting times of 50 and 25 s on peak and background, respectively.

Recalculation of mineral formulae

K-richterite analyses from both simplified and natural bulk compositions were recalculated from the oxide wt % assuming 23 oxygens, stoichiometric OH and $Fe_{tot} = Fe^{2+}$. In this case cation sums are usually very close to

Table 3: Average analyses of K-richterite

Experiment:	Ma76s	Ma86s	Ma64s	Ma62s	Ma96s	Ma99s	Ma106s
P (GPa):	6·5	6·5	7·0	8·0	8·0	9·0	8·0
T (°C):	800	850	1100	1100	1300	1100	1200
Capsule:	Pt_{100}	Pt_{100}	Pt_{100}	Pt_{100}	Pt_{100}	Pt_{100}	Pt_{100}
No. of analyses:	4	5	6	7	10	4	5
SiO_2	56·5(4)	55·9(3)	56·3(4)	55·8(3)	56·2(4)	56·3(6)	55·6(4)
Al_2O_3	2·9(2)	2·4(1)	3·0(2)	2·1(1)	2·1(1)	1·4(1)	1·9(1)
MgO	23·7(2)	23·9(2)	24·0(3)	24·2(2)	24·2(3)	24·0(2)	24·0(2)
CaO	7·4(2)	7·5(1)	7·2(1)	7·7(1)	7·5(2)	6·9(2)	7·4(1)
Na_2O	4·1(2)	3·5(1)	3·5(1)	2·8(0)	2·4(1)	2·4(1)	2·3(1)
K_2O	4·4(2)	5·1(1)	5·4(1)	6·1(1)	6·8(2)	7·0(1)	6·9(1)
H_2O	2·2(0)	2·2(0)	2·2(0)	2·2(0)	2·2(0)	2·2(0)	2·2(0)
Σ	101·3(6)	100·5(3)	101·8(6)	100·9(4)	101·4(4)	100·1(7)	100·3(6)
Si	7·72(2)	7·73(2)	7·69(2)	7·72(2)	7·74(3)	7·85(2)	7·75(2)
Al	0·47(3)	0·40(2)	0·48(3)	0·35(1)	0·35(2)	0·23(1)	0·32(1)
Mg	4·84(3)	4·92(3)	4·89(5)	4·99(2)	4·98(5)	4·98(1)	4·99(3)
Ca	1·09(3)	1·11(2)	1·07(1)	1·14(2)	1·10(3)	1·03(3)	1·11(2)
Na	1·10(5)	0·94(2)	0·93(2)	0·75(1)	0·63(2)	0·65(1)	0·63(1)
K	0·77(3)	0·90(1)	0·95(1)	1·08(2)	1·20(3)	1·25(2)	1·22(1)
Σ	15·98(2)	15·99(1)	16·01(3)	16·02(2)	16·00(2)	15·98(3)	16·02(2)
K/(K + Na)	0·41(2)	0·49(1)	0·50(1)	0·59(1)	0·65(1)	0·66(1)	0·66(1)

16·00. Because of the uncertainty of individual microprobe analyses, cation sums up to 16·05 were accepted as representative. Cations were assigned to structural positions as recommended by Leake (1978) [revised Leake *et al.* (1997)]. In case of Σ(Mg + Ca + Na) on M(4) < 2·0, K was assigned to M(4) to make KK-richterite component. Phlogopite was recalculated to 11 oxygens and stoichiometric OH. In the case where Σ(Si + Al) < 4, Fe^{3+} was added to the tetrahedral cations to bring the sums up to 4·0.

RESULTS OF THE EXPERIMENTS

Petrography

In both the simplified and the natural lherzolite system, mineral phases form euhedral to subhedral grains ≥10–20 μm in diameter except for grains of clinopyroxene and phlogopite, which rarely exceed 5–10 μm in size (Fig. 2). At temperatures <1100°C, the average grain size decreases rapidly and clinopyroxene grains may become too small (<5 μm) to be analysed with the microprobe. Garnets are typically poikiloblastic and contain numerous inclusions of clinopyroxene and/or olivine. At run durations >24 h, olivine often forms grain aggregates with perfect 120° triple point junctions. In run Ma80s orthopyroxene is absent and instead, coexisting omphacitic and diopsidic clinopyroxene can be texturally distinguished. The Al-poor clinopyroxene grains form aggregates of tiny, needle-like crystals, whereas the Al-rich ones are blocky isolated crystals that do not exceed 5 μm in length. Although the textures of the Al-poor clinopyroxenes would be consistent with a quench origin, these clinopyroxenes are not associated with K-rich phases and, therefore, are considered a stable phase coexisting with omphacite. In cases where quench could be identified, the quench phases were always K rich.

The phase distribution within individual charges is often inhomogeneous. Quenched fluid is typically concentrated at the capsule bottom along with olivine in low-temperature runs (e.g. Ma76, Ma86). Possible explanations for the concentration of olivine would be incongruent dissolution of phlogopite at subsolidus conditions or grain coarsening in a *T* gradient. Modal amounts of garnet may also strongly increase towards the capsule bottom. A similar, but less pronounced increase can be observed for clinopyroxene. Unlike the H_2O-rich peralkaline KNCMASH system investigated by Konzett *et al.* (1997), the high-temperature breakdown of K-richterite in the H_2O-poorer subalkaline KNCMASH system does not produce easily recognizable segregated melt. Instead, melt forms numerous small

Table 3: continued

Experiment:	PU620	PU633	PU638	PU643	PU649	Average composition	
P (GPa):	7·0	6·5	6·5	8·0	8·0	of K-richterite[1]	
T (°C):	1100	1100	1100	1100	1200	from PKP	from MARID
Capsule:	Pt_{100}	Pt_{100}	Pt_{100} + C	Pt_{100} + C	Pt_{100} + C		
No. of analyses:	8	4	8	7	3	69	53
SiO_2	55·5(3)	54·5(2)	55·7(5)	55·8(4)	55·5(1)	55·50	54·76
TiO_2	0·2(0)	0·2(0)	0·2(0)	0·1(0)	0·2(0)	0·41	0·64
Al_2O_3	2·2(1)	2·6(1)	2·5(1)	1·3(1)	1·2(0)	0·97	1·02
Cr_2O_3	0·3(0)	0·4(0)	0·4(1)	0·3(0)	0·2(1)	0·47	0·10
MgO	22·3(1)	22·8(1)	22·6(2)	22·8(2)	22·0(2)	22·74	21·69
FeO*	2·9(3)	2·8(2)	2·3(1)	2·1(1)	2·0(3)	2·34	3·95
MnO	<0·05	<0·05	<0·05	<0·05	<0·05	n.d.	n.d.
CaO	6·4(1)	6·8(2)	6·8(1)	6·2(1)	6·2(2)	6·64	6·86
Na_2O	3·4(1)	3·3(2)	3·5(1)	3·4(1)	3·4(1)	3·86	3·52
K_2O	5·9(1)	5·6(1)	5·5(0)	5·7(1)	6·1(1)	4·68	4·62
H_2O	2·2(0)	2·2(0)	2·2(0)	2·1(0)	2·1(1)	2·13	2·11
Σ	101·6(4)	101·4(3)	101·9(7)	99·9(9)	99·0(5)	99·74	99·27
Si	7·71(2)	7·60(1)	7·69(2)	7·84(1)	7·87(1)	7·804	7·787
Ti	0·02(0)	0·02(0)	0·02(0)	0·01(1)	0·02(0)	0·043	0·068
Al	0·37(2)	0·43(1)	0·41(1)	0·21(1)	0·21(1)	0·161	0·171
Cr	0·04(1)	0·05(0)	0·05(1)	0·03(0)	0·03(1)	0·052	0·011
Mg	4·63(2)	4·75(2)	4·65(3)	4·77(2)	4·67(2)	4·766	4·597
Fe	0·34(3)	0·33(2)	0·27(2)	0·25(1)	0·24(3)	0·275	0·470
Ca	0·96(2)	1·01(3)	1·01(1)	0·94(2)	0·94(4)	1·000	1·045
Na	0·91(2)	0·88(4)	0·93(2)	0·93(2)	0·94(2)	1·052	0·971
K	1·04(2)	0·99(2)	0·97(1)	1·02(0)	1·10(2)	0·839	0·838
Σ	16·04(2)	16·08(4)	16·02(2)	16·01(1)	16·01(2)	15·992	15·958
K/(K + Na)	0·53(1)	0·53(1)	0·51(1)	0·53(1)	0·54(0)	0·444	0·463
X_{Mg}	0·93(1)	0·94(0)	0·94(0)	0·91(0)	0·95(1)	0·945	0·907
ppm Ni	889(110)	820(98)	776(156)	717(29)	n.d.	n.d.	n.d.

Amphibole formulae recalculated to 23 oxygens + stoichiometric OH; numbers in parentheses denote 1σ standard deviation. [1]Average composition of K-richterite from phlogopite–K-richterite peridotites (PKPs) and mica–amphibole–rutile–ilmenite–diopside (MARID) xenoliths reported by Erlank *et al.* (1987, table II); a range of amphibole compositions has been given by Erlank *et al.* (1987, table I).

pools that contain K-rich quench phases, dispersed in the matrix. This feature makes the modal amounts of quench phases impossible to estimate in runs Ma100s and Ma101s. In the natural lherzolite system the breakdown of K-richterite occurs without formation of any detectable quench. Instead, X-ray mapping reveals that K, possibly deposited as extremely fine-grained quench, is dispersed along the interface between the experimental charge and the graphite capsule.

Chemical homogeneity of the phases

In both the simplified and the natural systems there is no systematic difference in the composition of phases analysed at the bottom and the top of individual experimental charges. With the exception of large (~20 μm or larger) garnet and K-richterite grains, no zoning within individual crystals can be observed. Garnets and clinopyroxenes, however, in part show considerable scatter in their Cr contents, which is ascribed to random inclusions of Cr_2O_3 remnants from the starting material. Most large garnet grains in both the simplified and the natural systems show Al- and Ca-rich cores. In the natural system some amphibole grains show cores distinctly lower in Al and Ca compared with rims. Both garnets and amphiboles show 5–10 μm wide rims of constant composition, which are thought to represent the equilibrium

Table 4: Average analyses of phlogopite

Experiment:	Ma60s	Ma85s	Ma63s	Ma81s	Ma64s	Ma62s	Ma83s	Ma86s
P (GPa):	4·0	5·0	6·0	6·5	7·0	8·0	6·5	6·5
T (°C):	1100	1100	1100	1100	1100	1100	950	850
Capsule:	Pt_{100}	Pt_{100}	Pt_{100}	Pt_{100}	Pt_{100}	Pt_{100}	Pt_{100}	Pt_{100}
No. of analyses:	4	8	5	7	5	4	5	3
SiO_2	42·1(3)	42·9(3)	44·4(2)	44·3(4)	45·3(7)	45·2(5)	44·0(4)	44·5(4)
Al_2O_3	15·6(1)	13·7(3)	12·8(1)	12·2(3)	12·0(5)	11·6(1)	11·9(1)	11·6(2)
MgO	27·8(2)	28·5(3)	28·7(2)	28·7(3)	29·1(1)	29·1(4)	28·6(2)	29·3(2)
CaO	<0·05	0·1(0)	<0·05	0·1(0)	<0·05	0·1(0)	<0·05	<0·05
Na_2O	0·5(1)	0·2(0)	0·2(0)	0·1(0)	0·1(0)	0·1(0)	0·1(0)	0·1(0)
K_2O	9·9(0)	10·2(1)	10·5(1)	10·4(2)	10·3(1)	10·6(2)	10·6(1)	10·2(1)
H_2O	4·4(0)	4·3(0)	4·4(0)	4·3(0)	4·4(0)	4·4(0)	4·3(0)	4·4(0)
Σ	100·3(5)	99·8(4)	101·0(4)	100·2(9)	101·3(6)	101·0(4)	99·6(4)	100·2(2)
Si	2·89(1)	2·96(1)	3·03(1)	3·05(1)	3·08(3)	3·09(3)	3·05(1)	3·06(2)
Al	1·27(1)	1·11(3)	1·03(1)	0·99(2)	0·96(4)	0·93(1)	0·97(1)	0·94(2)
Mg	2·84(2)	2·93(3)	2·92(2)	2·94(2)	2·94(1)	2·96(3)	2·96(2)	3·00(2)
Na	0·07(1)	0·03(0)	0·02(0)	0·02(0)	0·01(0)	0·01(0)	0·02(0)	0·02(0)
K	0·87(1)	0·90(1)	0·91(1)	0·92(1)	0·89(1)	0·92(2)	0·93(1)	0·90(0)
Σ	7·94(1)	7·94(1)	7·91(1)	7·92(2)	7·89(2)	7·91(3)	7·93(1)	7·92(1)
K/(K + Na)	0·93(1)	0·97(0)	0·97(0)	0·98(0)	0·99(0)	0·99(0)	0·98(0)	0·98(0)

garnet and amphibole composition at prevailing *P* and *T*. Average temperatures derived from diopside solid solution in enstatite as calibrated by Brey & Köhler (1990) are in good agreement with actual run temperatures (see Table 2), indicating that exchange reactions as fast as $CaMg_{-1}$ in pyroxene reached equilibrium.

Phase relations in KNCMASH

In the subalkaline KNCMASH system K-richterite is stable at pressures >6·0 GPa (Figs 2a and 3; Table 2). Below the K-richterite-in curve, the stable assemblage is phlogopite + clinopyroxene + orthopyroxene + garnet + fluid (Figs 2b and 3). Olivine joins the assemblage at pressures close to the K-richterite-in curve. The position of the K-richterite-in reaction curve was located between 6·0 and 6·5 GPa at 800°C, and between 6·5 and 7·0 GPa at 1100°C. Hence, the reaction has a positive slope with $dP/dT < 3{\cdot}3 \times 10^{-3}$ GPa/K.

In the presence of orthopyroxene as a possible reactant phase, the changes of mineral assemblage associated with the appearance of K-richterite are consistent with a reaction phlogopite + clinopyroxene + orthopyroxene = amphibole + garnet + olivine + fluid as initially proposed by Sudo & Tatsumi (1990). The high-temperature stability limit of K-richterite is reached between 1300 and 1400°C at 8·0 GPa, and at <1300°C at 7·0 GPa amphibole breakdown produces an anhydrous lherzolite assemblage garnet + olivine + clinopyroxene + orthopyroxene. The fine-grained interstitial quench material found in runs Ma100s and Ma101s is interpreted as quenched melt. Because of the surplus of phlogopite with respect to orthopyroxene, phlogopite coexists with amphibole between 7·0 and 8·0 GPa at 1100°C. Phlogopite finally breaks down in the absence of orthopyroxene between 8·0 and 9·0 GPa at 1100°C. This is accompanied by an abrupt increase of K p.f.u. in the amphibole, with a resulting KK-richterite component. The schematic reaction is

$$\text{phlogopite} + \text{clinopyroxene}_{ss} = \text{KK-richterite}_{ss} + \text{garnet}_{ss} + \text{olivine} + \text{fluid}. \quad (3)$$

Phlogopite breakdown between 1100 and 1200°C at 8·0 GPa again produces KK-richterite component in amphibole and is also responsible for the reappearance of orthopyroxene in subsolidus run Ma96s (see Fig. 3). The upper *T* stability of K-richterite with KK-richterite solid solution at 8·0 GPa is reached between 1300 and 1400°C. Under these conditions amphibole breaks down

Table 4: continued

Experiment:	PU624	PU633	PU654
P (GPa):	6·0	6·5	6·0
T (°C):	1100	1100	1100
Capsule:	Pt_{100}	Pt_{100}	Pt_{100} + C
No. of analyses:	5	5	5
SiO_2	41·7(7)	43·5(4)	43·0(4)
TiO_2	0·2(0)	0·1(0)	0·6(1)
Al_2O_3	11·7(7)	10·6(2)	12·0(1)
Cr_2O_3	0·3(0)	0·2(0)	0·2(0)
FeO	4·3(6)	3·4(3)	3·1(1)
Fe_2O_3	0·9(4)	1·8(3)	—
MnO	<0·05	<0·05	<0·05
MgO	25·6(2)	26·7(3)	25·9(3)
CaO	<0·05	<0·05	0·1(0)
Na_2O	0·1(0)	0·1(0)	0·2(0)
K_2O	10·6(0)	10·5(2)	10·6(1)
H_2O	4·2(0)	4·3(0)	4·3(0)
Σ	99·9(4)	101·4(6)	99·9(5)
Si	2·97(5)	3·04(1)	3·02(1)
Ti	0·01(0)	0·01(0)	0·03(1)
Cr	0·02(0)	0·01(0)	0·01(0)
Al	0·98(6)	0·87(0)	0·99(1)
Fe^{2+}	0·26(3)	0·20(2)	0·18(0)
Fe^{3+}	0·05(2)*	0·09(1)*	—
Mg	2·72(2)	2·77(2)	2·72(3)
Ca	—	—	0·01(0)
Na	0·01(0)	0·01(0)	0·02(0)
K	0·96(1)	0·93(2)	0·95(1)
Σ	7·98(2)	7·95(2)	7·93(1)
K/(K + Na)	0·99(0)	0·99(0)	0·98(0)
$X_{Mg}(Fe_{tot})$	0·90(1)	0·90(0)	0·94(0)
$X_{Mg}(Fe^{2+})$	0·91(1)	0·93(1)	0·94(0)
ppm Ni	1558(122)	1442(200)	n.d.

Phlogopite formulae recalculated to 11 oxygens + stoichiometric OH.
*Fe^{2+} was converted to Fe^{3+} so that Σ(Si + Al + Fe^{3+}) = 4·00 on the T-sites.

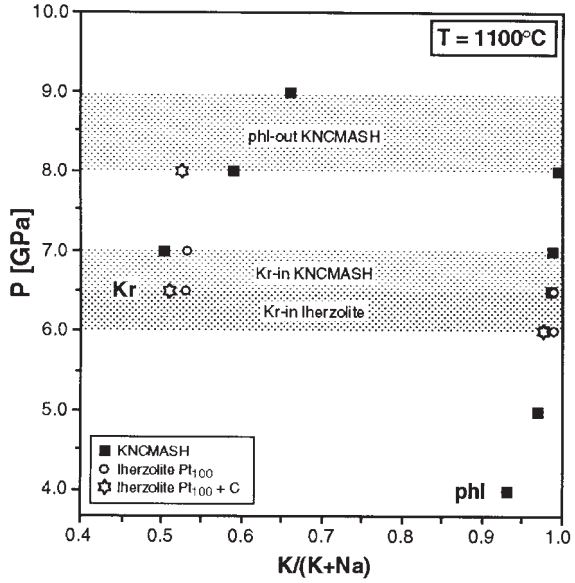

Fig. 5. K/(K + Na) ratios of phlogopite and K-richterite as a function of *P* at a constant temperature of 1100°C for runs in the KNCMASH and the natural lherzolite system (inset lower left). Shaded bands denote the pressure of K-richterite-in and phlogopite-out reactions in KNCMASH and the natural lherzolite system. Individual data points represent an average of several analyses (see Tables 3 and 4). Error bars are less than or equal to the size of plot symbols.

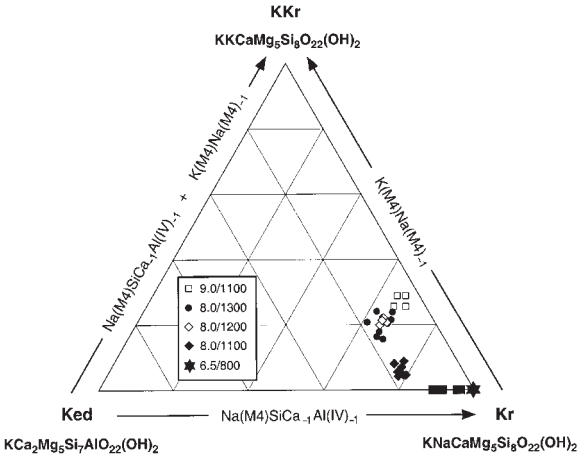

Fig. 6. Composition of amphibole in KNCMASH in terms of K-edenite, K-richterite and KK-richterite endmembers. Arrows denote exchange vectors for transformation of the amphibole endmembers. Mol % KK-richterite and K-richterite based on K(M4) and Na(M4), respectively; mol % K-edenite based on remaining Ca(M4).

to form a lherzolitic assemblage plus small amounts of fine-grained quench products.

Phase relations in the natural lherzolite system

As opposed to KNCMASH, no free fluid phase is present in the natural lherzolite system below the *P–T* conditions of the K-richterite-in curve, and the influence of Fe has to be considered. The stability of K-richterite in the lherzolite system is shifted slightly towards lower pressures compared with KNCMASH. K-richterite first appears and coexists with phlogopite at 6·5 GPa. At 1100°C, the pressure interval of coexisting phlogopite + amphibole is <1·0 GPa (Fig. 4). The shift of the K-richterite-in curve probably reflects partitioning of Fe^{2+} into garnet

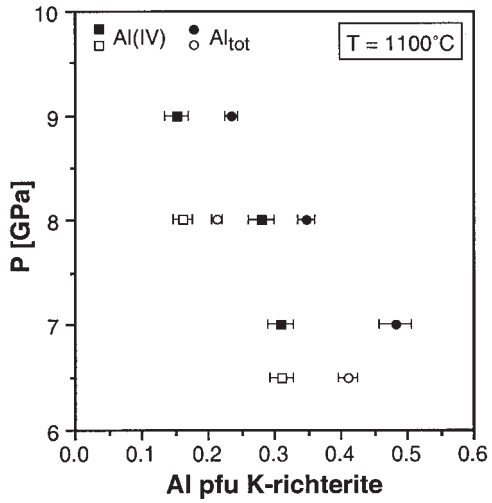

Fig. 7. Al contents of K-richterite as a function of P at constant T in KNCMASH (filled symbols) and in the natural lherzolite system using graphite capsules (open symbols). Individual data points represent an average of several analyses per run (Table 3).

which is part of the product assemblage of phlogopite breakdown. The persistence of phlogopite to 6·5 GPa is ascribed to a high Fe^{3+}/Fe^{2+} ratio in the Pt capsules, which stabilizes phlogopite with respect to amphibole. This assumption is supported by unusually high forsterite contents of coexisting olivine and pronounced tetrahedral cation deficits in phlogopite analyses when normalized to 11 oxygens and stoichiometric OH. To reduce Fe^{3+} in the experimental charges, experiments were rerun at 1100°C using double capsules with an inner graphite liner. This led to the disappearance of phlogopite at 6·5 GPa and 1100°C along with a significant change in the mineral compositions. At 8·0 GPa K-richterite disappears between 1200 and 1300°C. The K-richterite breakdown does not produce optically [back-scattered electron (BSE) and secondary electron (SE) imaging] detectable quench phases nor is there any significant change in the composition of lherzolite phases between 1100 and 1300°C. At 9·5 GPa no solid hydrous potassic phase was found at 1200 and 1300°C regardless of whether phlogopite or K-richterite-bearing starting material was used. X-ray mapping revealed that within the experimental charge K is concentrated in clinopyroxene and to a smaller degree dispersed along grain boundaries. The highest K concentration was found along grain boundaries of graphite grains within an ~20 μm wide zone at the interface between graphite capsule and experimental charge. The complete absence of K-richterite in runs at 9·5 GPa would imply a negative slope of the reaction that defines the high-temperature breakdown of K-richterite, opposite to the curvature observed in the synthetic KNCMASH system. A possible explanation for this discrepancy is that, in the natural system, increasing oxidation of graphite forms CO_2 with increasing pressure and temperature. This would reduce the activity of H_2O in the fluid and destabilize K-richterite, and possibly form trace amounts of alkaline CO_2-rich fluids or melts (e.g. Sweeney, 1994).

Mineral chemistry

Amphibole

Amphiboles in both the KNCMASH and the lherzolite systems are K-richterites (see Leake, 1978; revised Leake *et al.*, 1997). The major chemical variations are an increase in K and K/(K + Na) and a decrease in Na with increasing pressure at constant temperature (Fig. 5,

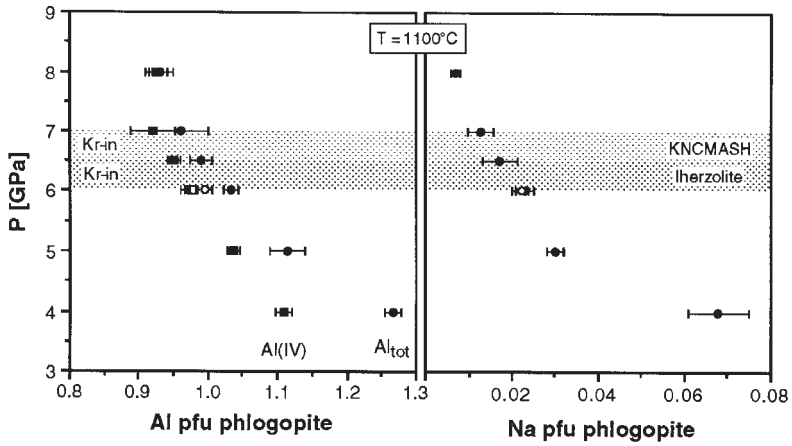

Fig. 8. Al and Na contents of phlogopite as a function of P at constant T in KNCMASH (filled symbols) and in the natural lherzolite system using graphite capsules (open symbols). Shaded bands denote the P range of K-richterite-in in KNCMASH and the natural lherzolite system. Individual data points represent an average of several analyses per run (Table 4).

Table 5: Average and representative analyses of clinopyroxene

Experiment:	Ma80s		Ma83s	Ma60s	Ma85s	Ma63s	Ma81s	Ma64s
P (GPa):	6·0		6·5	4·0	5·0	6·0	6·5	7·0
T (°C):	800		950	1100	1100	1100	1100	1100
Capsule:	Pt_{100}		Pt_{100}	Pt_{100}	Pt_{100}	Pt_{100}	Pt_{100}	Pt_{100}
	omphacitic	diopsidic						
No. of analyses:	5	7	8	5	7	13	5	8
SiO_2	58·0(8)	56·1(8)	56·9(4)	56·2(3)	56·2(5)	56·6(2)	56·5(1)	56·3(3)
Al_2O_3	16·6(2)	3·7(1)	4·7(1)	4·5(3)	4·0(4)	5·0(3)	4·5(2)	4·1(5)
MgO	8·0(2)	16·8(5)	17·2(9)	18·6(4)	18·6(4)	17·5(5)	18·0(5)	17·8(3)
CaO	9·6(2)	21·8(2)	19·5(9)	20·1(3)	20·0(4)	17·8(7)	19·1(4)	18·7(8)
Na_2O	9·3(1)	2·3(9)	2·9(6)	1·9(1)	2·1(2)	3·0(2)	2·7(1)	2·5(3)
K_2O	0·2(1)	0·2(1)	0·1(0)	0·1(0)	0·1(0)	0·1(0)	0·1(0)	0·2(1)
Σ	101·8(6)	100·8(10)	101·3(5)	101·4(1)	101·0(7)	100·0(3)	100·9(2)	99·7(5)
Si	1·70(1)	1·99(1)	1·99(0)	1·96(1)	1·97(1)	2·00(0)	1·98(0)	2·00(0)
Al	0·66(6)	0·15(5)	0·19(4)	0·19(1)	0·17(1)	0·21(1)	0·19(1)	0·17(2)
Mg	0·41(8)	0·88(3)	0·90(5)	0·97(2)	0·97(2)	0·92(3)	0·94(3)	0·94(2)
Ca	0·35(6)	0·83(8)	0·73(4)	0·75(1)	0·75(1)	0·67(3)	0·72(1)	0·71(3)
Na	0·61(6)	0·16(6)	0·20(4)	0·13(1)	0·14(1)	0·20(1)	0·18(1)	0·18(2)
K	0·01(1)	0·01(0)	0·01(0)	0·01(0)	0·01(0)	0·01(0)	0·01(0)	0·01(0)
Σ	4·01(2)	4·02(1)	4·01(1)	4·01(1)	4·02(1)	4·00(0)	4·02(1)	4·01(0)

Experiment:	Ma62s	Ma106s	Ma101s		Ma96s	Ma99s	Ma100s
P (GPa):	8·0	8·0	7·0		8·0	9·0	8·0
T (°C):	1100	1200	1300		1300	1100	1400
Capsule:	Pt_{100}	Pt_{100}	Pt_{100}		Pt_{100}	Pt_{100}	Pt_{100}
No. of analyses:	6	5	cpx1	cpx2	4	5	6
SiO_2	56·7(3)	56·8(5)	56·2	56·3	57·0(8)	55·8(3)	57·1(5)
Al_2O_3	2·8(2)	2·8(1)	3·8	3·9	3·1(2)	2·9(2)	3·6(3)
MgO	19·3(3)	19·4(6)	20·4	19·6	21·5(7)	19·8(3)	22·0(1)
CaO	21·0(5)	20·1(4)	18·1	18·1	17·1(1)	19·8(5)	16·1(1)
Na_2O	1·6(1)	1·6(1)	2·1	2·4	1·8(1)	1·7(1)	2·0(1)
K_2O	0·1(0)	0·3(1)	0·2	0·1	0·4(1)	0·4(0)	0·3(1)
Σ	101·5(5)	101·1(7)	100·7	100·4	100·9(9)	100·5(4)	101·2(3)
Si	1·99(0)	1·99(0)	1·97	1·98	1·99(1)	1·98(1)	1·98(1)
Al	0·11(1)	0·11(1)	0·16	0·16	0·13(1)	0·12(1)	0·15(1)
Mg	1·01(2)	1·02(2)	1·07	1·03	1·12(2)	1·04(1)	1·14(5)
Ca	0·79(2)	0·76(2)	0·68	0·68	0·64(4)	0·75(2)	0·60(6)
Na	0·11(1)	0·11(0)	0·14	0·16	0·12(1)	0·12(1)	0·14(1)
K	0·01(0)	0·02(0)	0·01	0·01	0·02(0)	0·02(0)	0·01(0)
Σ	4·01(0)	4·01(1)	4·02	4·02	4·02(0)	4·03(1)	4·02(1)

Table 3). These effects are more pronounced in KNCMASH than in the natural system. Maximum observed K contents in the KNCMASH system are 1·25 ± 0·02 (n = 4) K p.f.u. at 9·0 GPa and 1100°C, equivalent to 27 mol % of $KKCaMg_5Si_8O_{22}(OH)_2$ component (Fig. 6). In the natural system K contents are lower, with a maximum of 1·10 ± 0·02 (n = 3) K p.f.u. at 8·0 GPa and 1200°C, as a result of the considerably

Experiment:	PU624	PU633	PU620	PU654	PU638	PU643	PU647
P (GPa):	6·0	6·5	7·0	6·0	6·5	8·0	8·0
T (°C):	1100	1100	1100	1100	1100	1100	1400
Capsule:	Pt_{100}	Pt_{100}	Pt_{100}	Pt_{100} + C	Pt_{100} + C	Pt_{100} + C	Pt_{100} + C
No. of analyses:	5	5	4	5	7	7	5
SiO_2	55·4(9)	55·2(1)	55·9(4)	55·9(3)	55·5(4)	55·6(4)	56·8(3)
TiO_2	0·1(1)	0·1(0)	0·1(0)	0·2(0)	0·2(1)	0·2(0)	0·1(1)
Al_2O_3	2·1(5)	2·3(3)	2·1(1)	3·2(3)	2·7(2)	2·7(3)	2·2(1)
Cr_2O_3	0·5(4)	1·3(3)	0·8(4)	0·8(2)	1·3(5)	1·1(4)	0·8(2)
FeO	5·5(8)	5·4(3)	5·2(5)	4·2(7)	3·2(3)	3·4(2)	4·3(2)
MnO	0·1(0)	<0·05	0·1(0)	0·1(0)	0·1(0)	<0·05	0·1(0)
MgO	17·6(9)	16·6(4)	17·6(1)	18·1(7)	17·8(7)	17·3(2)	21·5(4)
CaO	16·1(1)	16·4(3)	16·8(9)	16·1(3)	17·7(5)	17·3(5)	13·3(4)
Na_2O	2·7(7)	3·3(3)	2·6(4)	2·8(3)	2·6(2)	2·7(2)	2·0(1)
K_2O	0·1(0)	0·1(0)	0·1(0)	<0·05	<0·05	0·1(0)	0·1(0)
Σ	100·4(1)	100·9(4)	101·4(6)	101·5(5)	101·1(5)	100·5(7)	101·4(3)
Si	2·00(1)	1·99(1)	2·00(1)	1·98(1)	1·98(0)	1·99(0)	2·00(0)
Ti	—	—	—	0·01(0)	0·01(0)	—	—
Al	0·09(2)	0·10(1)	0·09(1)	0·13(1)	0·11(1)	0·12(1)	0·09(1)
Cr	0·01(1)	0·40(1)	0·02(1)	0·02(1)	0·04(1)	0·03(1)	0·02(1)
Fe^{2+}	0·17(2)	0·16(1)	0·16(1)	0·12(2)	0·10(1)	0·10(1)	0·13(1)
Mg	0·95(5)	0·89(2)	0·94(6)	0·95(3)	0·95(4)	0·92(1)	1·12(2)
Ca	0·62(5)	0·63(1)	0·64(3)	0·61(1)	0·67(2)	0·66(2)	0·50(2)
Na	0·19(5)	0·23(2)	0·18(3)	0·19(2)	0·18(1)	0·19(1)	0·14(1)
Σ	4·04(1)	4·05(0)	4·04(1)	4·03(1)	4·03(1)	4·03(0)	4·02(0)
X_{Mg}	0·85(2)	0·85(1)	0·856(17)	0·88(2)	0·91(0)	0·90(0)	0·90(0)

Clinopyroxene formulae recalculated to six oxygens.

lower bulk K content of the lherzolite. All analysed K-richterite grains contain small amounts of Al(IV) and Al(VI), both of which decrease with increasing *P* at constant *T* in both chemical systems (Fig. 7). This decrease can be explained by a reaction

$$4\ Ca_2Mg_5Si_8O_{22}(OH)_2 + 4\ Mg_2SiO_4 + 5\ Al_2Mg_{-1}Si_{-1} = 8\ CaMgSi_2O_6 + 5\ Mg_3Al_2Si_3O_{12} + 4\ H_2O \quad (4)$$

causing clinopyroxene and garnet growth at the expense of amphibole. Fe contents of amphiboles in the lherzolite system range between 2·1 and 2·6 wt % FeO, corresponding to X_{Mg} of 0·94–0·95 on the basis of Fe_{tot} = FeO. Total cation numbers of lherzolitic amphiboles in Pt capsule experiments are slightly higher than those in the KNCMASH and the lherzolite system experiments performed in graphite capsules (see Table 3), indicating the presence of some Fe^{3+}. All lherzolitic amphiboles contain minor Ti, Cr and Ni. TiO_2 and Cr_2O_3 contents are $\leq$0·20 and 0·43 wt %, respectively, whereas Ni contents range between 640 and 1110 ppm. The significance of Ni contents in phlogopite and K-richterite will be discussed below.

Phlogopite

Phlogopite in KNCMASH shows only minor deviations from the ideal endmember composition (Table 4). The principal chemical variations are an increase in K and K/(K + Na), and a decrease in Al and Na p.f.u. with pressure at constant temperature (Figs 5 and 8). These effects duplicate the behaviour of amphibole. The decrease in Al can be attributed to garnet- or clinopyroxene-forming reactions. Modal amounts of garnet and clinopyroxene were determined in runs at 4·0 GPa and 1100°C, and 6·0 GPa and 1100°C using image analysis in three areas for garnet and six areas for clinopyroxene at the bottom, the centre and the tip of the capsules. The selected areas have an edge length of 400–500 μm. Although garnet distribution is inhomogeneous, the

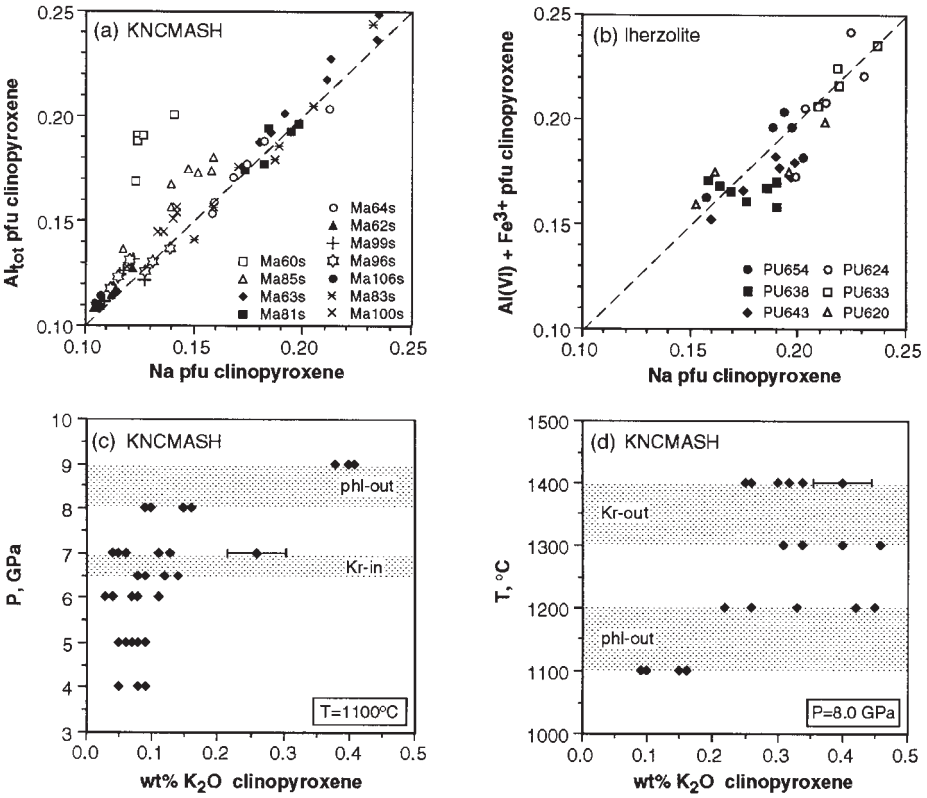

Fig. 9. Composition of clinopyroxene (a) in KNCMASH and (b) in the natural lherzolite system. Open and filled symbols in (b) denote clinopyroxene compositions from experiments performed in Pt and Pt + graphite capsules, respectively. Jadeite and jadeite + acmite compositions plot along the dashed lines. (c) and (d) K_2O contents of individual clinopyroxenes in KNCMASH across K-richterite-in and phlogopite-out reactions. Error bars denote 2σ error of an individual microprobe analysis.

modal amount strongly increases, from 7 to 26 vol %, from 4 to 9 vol % and from 4 to 7 vol % at the bottom, centre, and tip of the capsules between 4·0 and 6·0 GPa. The modal amount of clinopyroxene is much less variable, increasing from 21 to 25 vol %, from 19 to 25 vol % and from 18 to 26 vol % at the bottom, centre, and tip of the capsules within the same P range. This would be consistent with the assumption that garnet-forming reactions are mainly responsible for the Al decrease in phlogopite. For phlogopites with Al(IV) > 1·0 p.f.u. and in the presence of orthopyroxene, the relevant equilibrium is

$$2\ Mg_2Si_2O_6 + KMg_2Al[Al_2Si_2]O_{10}(OH)_2 = Mg_3Al_2Si_3O_{12} + KMg_3[AlSi_3]O_{10}(OH)_2 \quad (5)$$

which is a combination of two equilibria involving Tschermak exchange component (Thompson, 1982)

$$2\ Mg_2Si_2O_6 + Al_2Mg_{-1}Si_{-1} = Mg_3Al_2Si_3O_{12} \quad (5a)$$

$$KMg_2Al[Al_2Si_2]O_{10}(OH)_2 = KMg_3[AlSi_3]O_{10}(OH)_2 + Al_2Mg_{-1}Si_{-1}. \quad (5b)$$

At $P \geq 6{\cdot}0$ GPa, phlogopite has <1·0 Al p.f.u. In this case, garnet formation can involve montdorite component $KMg_{2\cdot5}[Si_4O_{10}](OH)_2$ (Seifert & Schreyer, 1971) in phlogopite (see Konzett *et al.*, 1997). Phlogopites formed in lherzolite runs using Pt capsules show tetrahedral cation deficits when normalized to 11 oxygens + stoichiometric OH. In runs PU624 and PU633 Σ(Si + Al) is 3·96 and 3·92, respectively. Fe^{3+} was used in these cases to fill the tetrahedral sites with a resulting $Fe^{3+}/(Fe^{3+} + Fe^{2+})$ of 0·16 and 0·31 (Table 4). In run PU654 (6·0 GPa and 1100°C, graphite capsule) no tetrahedral deficits are present and the mica composition is very similar to that in the KNCMASH system at identical P and T (see Table 4).

Clinopyroxene

Clinopyroxenes in KNCMASH are jadeite–diopside–enstatite solid solutions with a small Ca-Tschermak component. The latter rapidly decreases from 0·035 Al(IV) p.f.u. at 4·0 GPa and 1100°C to values well within the count statistical error of a microprobe analysis (Fig. 9, Table 5). Enstatite solid solution is constrained by the cpx–opx solvus (Brey *et al.*, 1990) and varies little with pressure between 10 and 14 mol % at 1100°C. At higher

Table 6: Average and representative analyses of garnet

Experiment:	Ma86s	Ma83s	Ma60s	Ma85s	Ma63s	Ma81s	Ma64s
P (GPa):	6·5	6·5	4·0	5·0	6·0	6·5	7·0
T (°C):	850	950	1100	1100	1100	1100	1100
Capsule:	Pt_{100}	Pt_{100}	Pt_{100}	Pt_{100}	Pt_{100}	Pt_{100}	Pt_{100}
No. of analyses:	3	6	5	7	3	5	11
SiO_2	45·1(3)	44·9(2)	44·1(4)	44·4(3)	44·6(3)	44·6(3)	44·5(2)
Al_2O_3	25·0(1)	25·3(3)	24·5(3)	24·6(3)	25·0(1)	25·2(4)	24·4(1)
MgO	27·1(1)	27·4(3)	25·8(3)	25·5(3)	27·0(2)	27·5(3)	27·5(3)
CaO	4·3(3)	3·9(2)	5·7(4)	6·9(2)	4·9(6)	3·8(3)	3·7(3)
Na_2O	0·1(0)	0·1(0)	<0·05	<0·05	<0·05	0·1(0)	0·1(0)
K_2O	<0·05	<0·05	<0·05	<0·05	<0·05	<0·05	<0·05
Σ	101·6(3)	101·7(4)	100·1(6)	101·5(4)	101·6(4)	101·3(3)	100·2(3)
Si	3·02(2)	3·00(1)	3·01(1)	3·00(1)	2·99(1)	2·99(2)	3·01(1)
Al	1·97(1)	1·99(2)	1·97(1)	1·95(2)	1·98(1)	2·00(3)	1·95(1)
Mg	2·71(1)	2·73(2)	2·62(2)	2·57(2)	2·69(3)	2·75(2)	2·78(3)
Ca	0·31(2)	0·28(2)	0·42(4)	0·50(2)	0·35(4)	0·27(2)	0·27(2)
Na	0·01(0)	0·01(0)	—	—	—	0·01(0)	0·01(0)
Σ	8·00(2)	8·00(1)	8·01(1)	8·02(1)	8·02(0)	8·01(1)	8·02(1)
Ca/(Ca + Mg)	0·10(1)	0·10(0)	0·14(1)	0·16(1)	0·12(1)	0·09(1)	0·09(1)

Experiment:	Ma101s	Ma62s	Ma106s	Ma96s	Ma100s	Ma99s
P (GPa):	7·0	8·0	8·0	8·0	8·0	9·0
T (°C):	1300	1100	1200	1300	1400	1100
Capsule:	Pt_{100}	Pt_{100}	Pt_{100}	Pt_{100}	Pt_{100}	Pt_{100}
No. of analyses:	5	5	8	5	5	5
SiO_2	44·4(4)	45·0(3)	45·6(4)	45·4(4)	45·3(1)	45·7(5)
Al_2O_3	24·1(4)	25·0(2)	24·1(6)	23·6(2)	24·0(2)	23·1(4)
MgO	27·3(3)	27·9(4)	27·6(3)	26·8(6)	28·3(3)	28·2(2)
CaO	3·7(3)	3·9(3)	4·3(3)	4·8(7)	4·0(2)	4·2(3)
Na_2O	0·1(0)	0·1(0)	0·1(0)	0·2(1)	0·1(0)	0·2(0)
K_2O	0·1(0)	<0·05	0·5(0)	0·1(0)	0·1(0)	0·1(1)
Σ	99·8(3)	101·9(2)	101·8(6)	100·8(8)	101·8(4)	101·6(1)
Si	3·02(2)	3·00(2)	3·04(2)	3·06(1)	3·02(0)	3·06(2)
Al	1·93(4)	1·97(2)	1·90(4)	1·88(2)	1·89(1)	1·82(4)
Mg	2·77(3)	2·77(4)	2·74(3)	2·70(4)	2·82(2)	2·82(1)
Ca	0·27(2)	0·28(2)	0·31(2)	0·35(5)	0·29(2)	0·30(2)
Na	0·01(0)	0·01(0)	0·01(0)	0·02(0)	0·01(0)	0·03(0)
Σ	8·02(1)	8·02(1)	8·01(2)	8·01(1)	8·04(0)	8·03(1)
Ca/(Ca + Mg)	0·09(1)	0·09(1)	0·10(1)	0·11(1)	0·09(1)	8·03(1)

temperatures, enstatite component increases, reaching 27 mol % at 8·0 GPa and 1400°C. Na in clinopyroxene increases with pressure to a maximum averaged value of 19 mol % jadeite at 6·5 GPa. At higher pressures, jadeite component is consumed by the amphibole-forming reaction and the re-partitioning of Na between amphibole and clinopyroxene decreases Na contents of clinopyroxene formed at pressures between 7·0 and 8·0 GPa. At 6·0 GPa and 1100°C two coexisting clinopyroxenes—diopside and omphacite—occur instead of orthopyroxene in the KNCMASH system. The diopside ranges in composition from $jad_7di_{91}cats_2$ to $jad_{21}di_{71}en_7cats_1$, whereas

Table 6: continued

Experiment:	PU624	PU633		PU620		PU654	PU638	PU643	PU647
P (GPa):	6·0	6·5		7·0		6·0	6·5	8·0	8·0
T (°C):	1100	1100		1100		1100	1100	1100	1400
Capsule:	Pt_{100}	Pt_{100}		Pt_{100}		Pt_{100} + C	Pt_{100} + C	Pt_{100} + C	Pt_{100} + C
No. of analyses:	6	ga1	ga2	ga1	ga2	4	4	6	5
SiO_2	42·0(6)	42·0	42·7	41·3	42·4	42·2(6)	42·1(5)	42·7(4)	44·0(2)
TiO_2	0·2(0)	0·2	0·2	0·2	0·2	0·3(0)	0·3(1)	0·3(1)	0·4(1)
Al_2O_3	23·6(6)	22·1	22·0	24·8	23·8	23·6(9)	23·6(4)	23·2(6)	20·7(1)
Cr_2O_3	0·7(4)	0·5	0·8	0·4	0·4	0·8(2)	1·0(3)	0·7(4)	1·9(4)
FeO	7·4(6)	7·4	7·7	7·4	7·2	7·6(6)	7·5(2)	8·4(2)	6·9(1)
MnO	0·2(0)	0·2	0·3	0·2	0·3	0·2(0)	0·2(0)	0·2(0)	0·1(0)
MgO	23·3(4)	23·6	22·5	21·8	23·1	22·8(7)	22·6(4)	22·0(4)	24·3(9)
CaO	3·9(1)	3·9	4·4	3·8	3·7	4·2(2)	3·9(1)	3·9(4)	3·2(3)
Na_2O	0·1(0)	<0·05	<0·05	<0·05	<0·05	0·1(0)	0·1(0)	0·1(0)	0·1(0)
Σ	101·6(8)	99·9	100·5	99·9	101·1	101·9(7)	101·3(7)	101·5(4)	101·7(9)
Si	2·92(2)	2·97	3·00	2·91	2·95	2·94(3)	2·94(2)	2·98(2)	3·05(3)
Ti	0·01(0)	0·01	0·01	0·01	0·01	0·02(0)	0·02(0)	0·01(1)	0·02(1)
Al	1·94(5)	1·84	1·83	2·06	1·96	1·93(6)	1·94(3)	1·91(4)	1·69(9)
Cr	0·04(2)	0·03	0·05	0·04	0·02	0·04(1)	0·06(1)	0·04(2)	0·10(3)
Fe^{2+}	0·43(3)	0·43	0·46	0·44	0·42	0·44(3)	0·44(1)	0·49(1)	0·40(6)
Mn	0·01(0)	0·01	0·02	0·02	0·02	0·01(0)	0·01(0)	0·01(0)	0·01(0)
Mg	2·42(3)	2·49	2·36	2·29	2·39	2·36(9)	2·35(3)	2·29(3)	2·51(8)
Ca	0·29(1)	0·30	0·33	0·29	0·27	0·32(1)	0·29(1)	0·29(3)	0·23(2)
Na	0·01(1)	—	—	—	—	0·01(0)	0·01(0)	—	0·01(1)
Σ	8·08(1)	8·08	8·05	8·03	8·04	8·06(2)	8·05(1)	8·03(1)	8·03(4)
X_{Mg}	0·85(1)	0·85	0·84	0·84	0·85	0·84(1)	0·84(0)	0·82(0)	0·86(2)

Garnet formulae recalculated to 12 oxygens.

omphacite ranges from $jad_{52}di_{41}en_3cats_4$ to $jad_{67}di_{29}en_2cats_2$ (Table 5). The system jadeite–augite shows complex subsolidus exsolution behaviour at low *T*–high *P* with two immiscible regions across which omphacite can coexist with sodic diopside or calcic jadeite (Rossi, 1988, and references therein). Coexisting clinopyroxenes have been reported from natural rocks (Droop *et al.*, 1990) and are known from experimental studies. Schmidt (1992) reported coexisting omphacite and sodic omphacite–augitic omphacite in a tonalitic bulk system between 1·7 and 3·6 GPa and 650°C. The presence of coexisting clinopyroxenes at temperatures as high as 800°C in this study probably reflects the high experimental pressure, which might shift the critical point of the immiscible region to higher temperatures compared with natural rocks (Carpenter & Smith, 1981) and/or the lack of Fe, and particularly Fe^{3+} in the subalkaline KNCMASH system.

Clinopyroxene in lherzolite experiments between 6·0 and 8·0 GPa show jadeite contents of 6–10 mol % and an acmite component from 4 to 9 mol % in graphite capsules and from 11 to 16 mol % in Pt capsules. The formation of amphibole decreases the jadeite component from 10 to 7 mol % between 6·0 and 6·5 GPa. Potassium contents of KNCMASH clinopyroxene in the presence of phlogopite are small with values <0·2 wt % K_2O (see Fig. 9). The breakdown of phlogopite at high pressures (phl → Kr) and high temperatures (phl → Kr + en) is accompanied by a significant increase of K_2O in the clinopyroxene that coexists with either K-richterite or melt–fluid. Such clinopyroxene displays up to 0·45 wt % K_2O (Fig. 9). Under very high pressure conditions, clinopyroxene in the lherzolite system contains between

Table 7: Average analyses of olivine

Experiment:	PU624	PU633	PU620	PU654	PU638	PU643	PU647	BRIAN 2*
P (GPa):	6·0	6·5	7·0	6·0	6·5	8·0	8·0	
T (°C):	1100	1100	1100	1100	1100	1100	1400	
Capsule:	Pt_{100}	Pt_{100}	Pt_{100}	Pt_{100} + C	Pt_{100} + C	Pt_{100} + C	Pt_{100} + C	
No. of analyses:	6	4	8	4	8	7	7	5
SiO_2	42·2(6)	41·5(4)	42·1(4)	41·2(5)	41·9(4)	40·8(6)	41·5(2)	41·1(4)
TiO_2	<0·05	<0·05	<0·05	<0·05	<0·05	<0·05	<0·05	<0·05
Al_2O_3	<0·05	<0·05	<0·05	<0·05	<0·05	<0·05	<0·05	<0·05
Cr_2O_3	0·1(0)	<0·05	0·1(0)	<0·05	<0·05	<0·05	<0·05	<0·05
FeO	6·5(2)	6·7(3)	6·6(2)	8·8(4)	8·2(3)	8·7(2)	8·3(1)	9·4(1)
MnO	0·1(0)	0·1(0)	0·1(0)	0·1(0)	0·1(0)	0·1(0)	0·1(0)	0·1(0)
MgO	52·8(3)	53·2(4)	52·6(4)	50·9(6)	51·7(5)	50·6(2)	50·6(3)	50·2(2)
CaO	0·1(0)	<0·05	0·1(0)	0·1(0)	<0·05	<0·05	0·1(0)	<0·05
Σ	102·0(5)	102·0(6)	101·8(6)	101·4(9)	102·2(5)	100·4(8)	101·1(5)	101·4(6)
Si	1·00(1)	0·98(0)	1·00(1)	0·99(1)	1·00(1)	0·99(1)	1·00(0)	0·99(0)
Fe^{2+}	0·13(0)	0·13(0)	0·13(0)	0·18(1)	0·16(1)	0·18(3)	0·17(0)	0·19(0)
Mn	—	0·01(0)	—	—	—	—	—	—
Mg	1·86(1)	1·88(0)	1·86(1)	1·82(1)	1·83(1)	1·83(4)	1·82(1)	1·81(1)
X_{Fo}	0·93(0)	0·93(3)	0·93(0)	0·91(0)	0·91(0)	0·91(2)	0·91(0)	0·90(0)
ppm Ni	2568(436)	2613(311)	2441(375)	n.d.	2585(346)	2714(700)	2246(328)	2997(369)

Olivine formulae recalculated to four oxygens.
*Composition of olivine in starting material BRIAN 2.

Table 8: Average analyses of orthopyroxene

Experiment:	Ma60s	Ma85s	Ma63s	Ma81s	Ma83s	Ma106s	Ma96s	Ma100s
P (GPa):	4·0	5·0	6·0	6·5	6·5	8·0	8·0	8·0
T (°C):	1100	1100	1100	1100	950	1200	1300	1400
Capsule:	Pt_{100}	Pt_{100}	Pt_{100}	Pt_{100}	Pt_{100}	Pt_{100}	Pt_{100}	Pt_{100}
No. of analyses:	7	9	10	9	5	8	8	6
SiO_2	59·6(3)	59·6(6)	60·1(3)	60·4(7)	60·5(5)	60·0(4)	59·9(6)	59·6(4)
Al_2O_3	2·3(3)	1·2(2)	1·1(3)	0·9(3)	0·5(2)	0·9(1)	1·4(4)	1·2(3)
MgO	39·1(4)	39·7(3)	39·3(3)	39·8(5)	39·8(3)	39·2(3)	38·2(5)	38·6(8)
CaO	0·8(1)	0·6(1)	0·5(1)	0·5(1)	0·2(0)	0·9(0)	1·4(2)	1·3(4)
Na_2O	0·1(0)	0·2(0)	0·2(0)	0·2(1)	0·1(0)	0·3(0)	0·5(1)	0·4(2)
K_2O	<0·05	<0·05	<0·05	<0·05	<0·05	<0·05	<0·05	0·1(0)
Σ	102·0(3)	101·6(7)	101·3(5)	101·9(9)	101·2(5)	101·3(6)	101·5(7)	101·2(4)
Si	1·96(1)	1·97(1)	1·99(1)	1·99(1)	2·00(1)	1·99(1)	1·98(1)	1·98(0)
Al	0·08(1)	0·05(1)	0·04(1)	0·03(1)	0·02(1)	0·04(0)	0·06(1)	0·05(1)
Mg	1·92(1)	1·95(1)	1·94(2)	1·95(2)	1·96(1)	1·93(1)	1·88(3)	1·91(3)
Ca	0·03(0)	0·02(0)	0·02(0)	0·02(0)	0·01(0)	0·03(0)	0·05(1)	0·04(1)
Na	0·01(1)	0·01(0)	0·01(0)	0·01(0)	0·01(0)	0·02(0)	0·03(1)	0·03(1)
Σ	4·00(0)	4·01(0)	4·00(1)	4·01(1)	3·99(0)	4·00(0)	4·00(1)	4·01(0)

Table 8: continued

Experiment:	PU624	PU633	PU620	PU654	PU638	PU643	PU647
P (GPa):	6·0	6·5	7·0	6·0	6·5	8·0	8·0
T (°C):	1100	1100	1100	1100	1100	1100	1400
Capsule:	Pt_{100}	Pt_{100}	Pt_{100}	Pt_{100} + C	Pt_{100} + C	Pt_{100} + C	Pt_{100} + C
No. of analyses:	6	5	3	5	6	4	4
SiO_2	58·8(3)	58·6(2)	58·4(3)	58·3(3)	59·3(4)	58·1(2)	58·9(4)
TiO_2	<0·05	<0·05	<0·05	0·1(0)	<0·05	<0·05	<0·05
Al_2O_3	0·8(4)	0·5(0)	0·5(1)	0·7(1)	0·4(0)	0·5(2)	0·9(4)
Cr_2O_3	0·3(1)	0·3(1)	0·2(1)	0·2(1)	0·3(0)	0·2(0)	0·3(0)
FeO	4·7(2)	4·8(4)	5·6(9)	6·4(1)	4·9(1)	5·2(4)	5·3(2)
MnO	0·1(0)	0·1(0)	0·1(0)	<0·05	0·1(0)	0·1(0)	0·1(0)
MgO	36·0(4)	36·6(4)	35·1(8)	34·9(8)	36·0(4)	35·6(2)	34·2(6)
NiO	0·1(0)	0·1(0)	n.d.	n.d.	0·1(0)	n.d.	0·1(0)
CaO	0·6(1)	0·5(1)	0·7(1)	0·8(1)	0·5(0)	0·5(1)	1·5(3)
Na_2O	0·2(0)	0·3(0)	0·3(0)	0·3(0)	0·2(0)	0·2(0)	0·5(0)
K_2O	<0·05	<0·05	<0·05	<0·05	<0·05	<0·05	<0·05
Σ	101·7(3)	101·8(3)	100·9(9)	101·7(3)	101·9(7)	100·5(5)	101·9(7)
Si	1·98(1)	1·97(0)	1·99(1)	1·98(0)	2·00(0)	1·99(1)	1·99(1)
Al	0·03(1)	0·02(0)	0·02(0)	0·03(0)	0·02(0)	0·02(1)	0·04(2)
Cr	0·01(0)	0·01(0)	0·01(0)	0·01(0)	0·01(0)	0·01(0)	0·01(0)
Fe^{2+}	0·13(0)	0·13(1)	0·16(3)	0·18(4)	0·14(0)	0·15(1)	0·15(1)
Mg	1·81(2)	1·84(1)	1·78(3)	1·77(3)	1·81(1)	1·81(1)	1·72(2)
Ca	0·02(0)	0·02(0)	0·03(0)	0·03(0)	0·02(0)	0·02(0)	0·06(1)
Na	0·02(0)	0·02(0)	0·02(0)	0·02(0)	0·01(0)	0·01(0)	0·03(0)
Σ	4·01(0)	4·02(0)	4·01(1)	4·01(0)	4·00(0)	4·01(1)	4·00(1)
X_{Mg}	0·93(0)	0·93(1)	0·92(2)	0·91(2)	0·93(0)	0·92(0)	0·92(0)

Orthopyroxene formulae recalculated to 6 oxygens.

0·05 and 0·10 wt % K_2O as a result of the much lower bulk contents of the natural starting material.

Garnet, olivine, and orthopyroxene

Garnet in KNCMASH is a binary pyrope–grossular solid solution with Ca/(Ca + Mg) decreasing with increasing pressure (Brey *et al.*, 1990) to 6·5 GPa. Within the K-richterite stability field, X_{Ca} remains constant to the highest pressure we studied. At 8·0 and 9·0 GPa individual garnet analyses typically show >3·0 Si p.f.u., with a maximum of 3·06 ± 0·02 Si p.f.u. at 9·0 GPa. Garnet compositions in the lherzolite system are constant between 6·0 and 8·0 GPa, with Mg/(Mg + Fe_{tot}) and X_{Ca} between 0·82 and 0·84, and 0·09 and 0·11, respectively (Table 6).

Olivine in the lherzolite system experiments with graphite capsules ranges between Fo_{91} and Fo_{92}, compositions very similar to those of olivine in BRIAN 2 (Table 7). Olivine formed in Pt capsules displays forsterite contents close to Fo_{93}. Ni contents of olivine are between 2000 and 3500 ppm, which is within the expected range for primary mantle olivines (Griffin *et al.*, 1989).

Orthopyroxene shows decreasing Mg-Tschermak and diopside components along with increasing Na with pressure and temperature (Table 8), constrained by the coexistence with garnet and clinopyroxene (Brey & Köhler, 1990; Brey *et al.*, 1990, and references therein).

DISCUSSION

Amphibole-forming reactions in Na-free and Na-bearing systems

Sudo & Tatsumi (1990) and Luth (1997) used an Na-free KCMASH system to assess the potential stability range of KK-richterite under upper-mantle *P–T* conditions. The KCMASH system is relevant to this study

Table 9: List of mineral endmembers, abbreviations and formulae used in this study

Mineral	Abbreviation	Formula
clinopyroxene	cpx	
diopside	di	$CaMgSi_2O_6$
eastonite		$KMg_2Al[Al_2Si_2O_{10}](OH)_2$
enstatite	en	$Mg_2Si_2O_6$
garnet	ga	
grossular	gross	$Ca_3Al_2Si_3O_{12}$
jadeite	jad	$NaAlSi_2O_6$
K-edenite	Ked	$KCa_2Mg_5[Si_7Al]O_{22}(OH)_2$
K-richterite	Kr	$KNaCaMg_5Si_8O_{22}(OH)_2$
KK-richterite	KKr	$KKCaMg_5Si_8O_{22}(OH)_2$
olivine	ol	Mg_2SiO_4
omphacite	omp	
orthopyroxene	opx	
phlogopite	phl	$KMg_3[AlSi_3O_{10}](OH)_2$
pyrope	py	$Mg_3Al_2Si_3O_{12}$
quenched fluid–melt	Q	
tremolite		$Ca_2Mg_5Si_8O_{22}(OH)_2$
Tschermak-vector		$Al_2Mg_{-1}Si_{-1}$

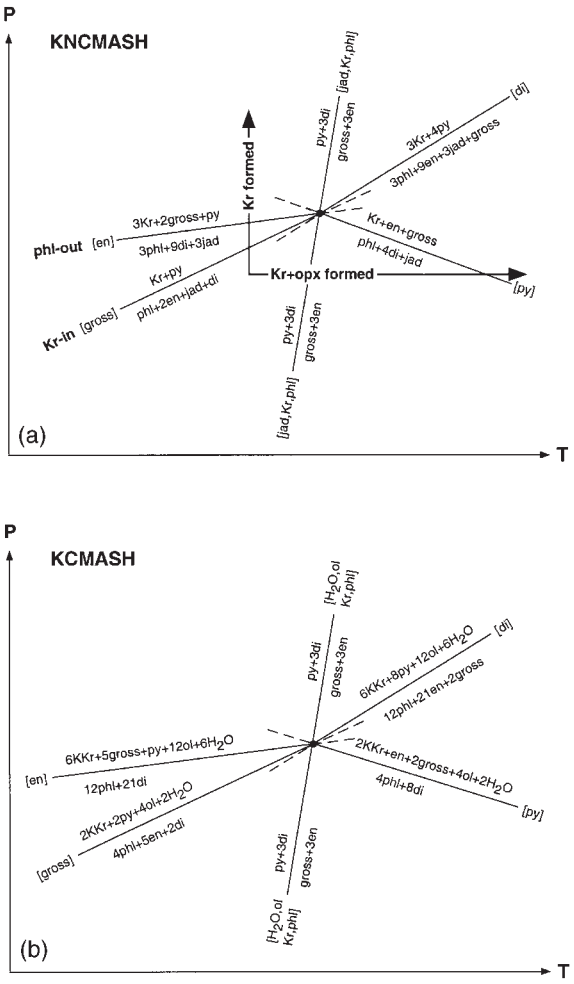

Fig. 10. Schematic phase relations in *P–T* space of clinopyroxene, orthopyroxene, garnet, olivine, phlogopite and amphibole using endmember mineral compositions (a) in KNCMASH and (b) in KCMASH. No CaMg solid solution was considered for garnet and no CaMg–NaAl solid solution was considered for clinopyroxene. The reactions with endmember garnet and clinopyroxene ([jad, Kr, phl] and [Kr, phl, ol, H_2O], respectively) are single isopleths that represent a particular garnet and clinopyroxene composition. (For abbreviations, see Table 9.) Arrows in (a) denote observed reactions towards high pressures (K-richterite formation) and high temperatures (K-richterite + orthopyroxene formation) observed in the experiments. Reactions are arranged to be consistent with a positive slope of the grossular-absent reaction and balanced using the REACTION program of Finger & Burt (1972).

because K-richterite in the KNCMASH system contains a significant KK-richterite component at very high pressures.

Phase relations and mineral assemblages found in the KNCMASH and KCMASH systems are shown in Fig. 10. Because endmember phlogopite and K-richterite have identical K/OH ratios, reactions in KNCMASH do not produce a free fluid (Fig. 10a). The grossular-absent reaction (Fig. 10a) corresponds to the K-richterite-forming reaction proposed by Luth *et al.* (1993). In Fig. 10a, H_2O is a phase component but not a phase, and $a(H_2O)$ defined by equilibria involving hydrous phases is less than $a(H_2O)$ of a pure water phase at the same P and T. According to Thompson (1983), H_2O-conserving reactions generally cannot be located in P–T space by direct experiments involving a free fluid, because the presence of H_2O as a phase shifts the bulk composition to a region in composition space not accessible to H_2O-conserving equilibria. In the KCMASH system the amphibole endmember is $KKCaMg_5Si_8O_{22}(OH)_2$, which is very close to $K_{1\cdot9}Ca_{1\cdot1}Mg_5[Si_{7\cdot9}Al_{0\cdot1}]O_{22}(OH)_2$ reported by Sudo & Tatsumi (1990). The higher K/OH ratio of KK-richterite compared with that of phlogopite requires that all phlogopite breakdown reactions that form KK-richterite must release H_2O (see Fig. 10b). If phlogopite and amphibole deviate from their endmember stoichiometry, the number of moles of H_2O produced during formation of 1 mol amphibole by phlogopite breakdown is ($K_{amphibole}$ p.f.u./$K_{phlogopite}$ p.f.u.) − 1. In Fig. 10b, the enstatite- and grossular-absent reactions are equivalents to the amphibole-forming reactions of Sudo & Tatsumi (1990).

The high Na content of K-richterite close to endmember composition and the resulting small difference in K/OH between K-richterite and phlogopite compared with KK-richterite and phlogopite require that only a small amount

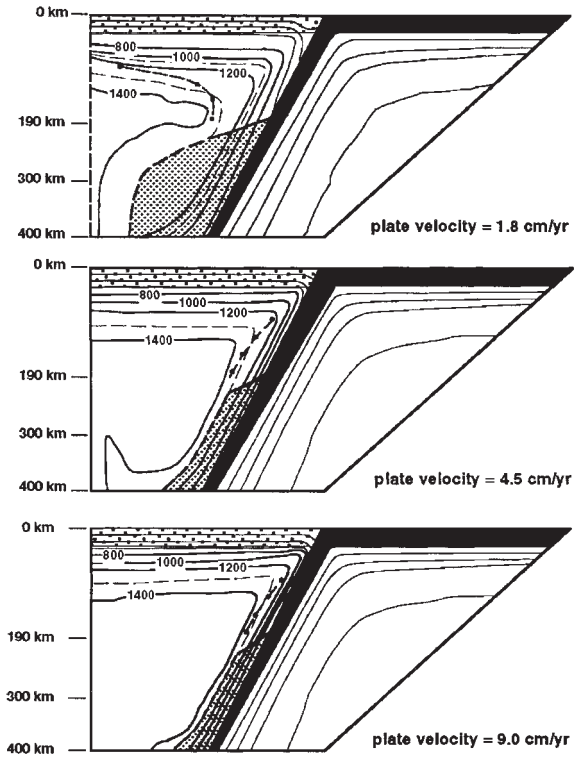

Fig. 11. Temperature distribution in the mantle wedge above a subducting slab according to the model of Davis & Stevenson (1992) for a subduction angle of 60° and three different subduction velocities. The shaded area in the wedge represents an approximate potential stability field of K-richterite as deduced from experiments of the present study. The upper T stability limit of K-richterite is thought to be at T < 1400°C as determined in the KNCMASH system and was (arbitrarily) placed at 1300°C in the absence of unambiguous evidence for K-richterite melting in the lherzolitic system (see text for discussion). The dashed line connecting dots is an approximate upper T stability limit for phlogopite in lherzolite extrapolated from experimental data of Wendlandt & Eggler (1980). Lines with numbers refer to isotherms and corresponding temperatures.

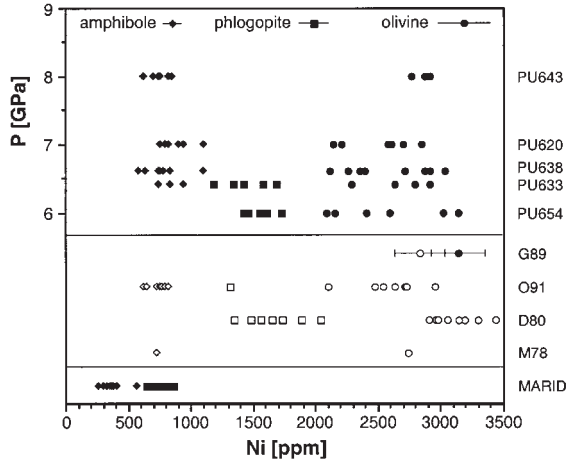

Fig. 12. Ni contents of amphibole, phlogopite and olivine from various mantle sources compared with experimentally produced Ni contents of K-richterite, phlogopite and coexisting olivine in the natural lherzolite system (PU numbers; see Table 2). G89, average Ni contents in olivine from diamond inclusions (●) and from garnet peridotites (○) reported by Griffin *et al.* (1989); O91, pargasitic amphiboles and coexisting phlogopite and olivine from spinel lherzolites (O'Reilly *et al.*, 1991); D80, primary textured phlogopites and coexisting olivine from harzburgitic and lherzolitic xenoliths (Delaney *et al.*, 1980); M78, pargasite and coexisting olivine in equilibrium with water-saturated liquid at 1·5 GPa and 1000°C (Mysen, 1978). K-richterite and phlogopite from MARID xenoliths were analysed by PIXE, all other analyses are by electron microprobe (Konzett, 1996). Error bars represent errors of individual microprobe analyses. Errors for PIXE analyses are smaller than the plotting symbols (Sweeney *et al.*, 1995).

of fluid is produced during K-richterite formation. The reaction cannot be strictly H_2O conserving because it is observed in the experiments (Thompson, 1983). The positive slope of the K-richterite-forming reaction in KNCMASH implies that H_2O is on the low-entropy–low-temperature side of the reaction. Although this is not a common feature of water-releasing reactions, it is typical of reactions that involve glaucophane (Holland, 1988). The negative slope of the KK-richterite-forming reaction, as suggested by Sudo & Tatsumi (1990) for the KCMASH system, resembles the slopes of calcic amphibole dehydration reactions, but it is not well constrained within the spacing of the experimental data points of Sudo & Tatsumi (1990) (see Fig. 3).

The stability of potassium amphibole in lherzolitic mantle

Subcontinental lithosphere

The P–T conditions defined by an average 40 mW/m^2 conductive continental shield geotherm (Pollack & Chapman, 1977) are outside the K-richterite stability field for the natural lherzolite system (Fig. 3). In regions of subcontinental mantle with a heat flow <40 mW/m^2, P–T conditions straddle the high-temperature corner of this amphibole stability field. Unless it is stabilized by F, K-richterite is probably not present in subcontinental mantle lherzolite. Foley (1991) showed that at 5·0 GPa, the T stability limit of K–F-richterite is increased by ~200°C compared with that of K–OH-richterite. However, phlogopites from metasomatized peridotites generally contain <1·0 wt % F (Delaney *et al.*, 1980; Smith *et al.*, 1980).

Subduction zone settings

Because subducting slabs are heat sinks, temperatures in the mantle wedge above a descending slab are anomalously cold compared with other mantle regions. Thermal models for subduction zones (e.g. Davis & Stevenson, 1992; Furukawa, 1993) predict steady-state temperatures of 800–1000°C at the slab–mantle interface,

with isotherms parallel to the subducting slab. *P–T* conditions in part of the mantle wedge are thus within the K-richterite stability field below a depth of ~180 km or 6 GPa. The mantle volume in which K-richterite is potentially stable varies with the spacing of isotherms. According to the theoretical model of Davis & Stevenson (1992), increasing subduction velocity leads to a hotter wedge with a tighter spacing of the isotherms. Therefore, fast subduction should reduce the mantle volume in which K-richterite is stable (Fig. 11). Different subduction angles and varying thickness of the slab, on the other hand, have little influence on the *T* distribution in the wedge in the model of Davis & Stevenson (1992).

Both phlogopite breakdown in peridotites dragged down along the slab–mantle interface and interaction between mantle peridotites and K-rich fluids or melts at pressures above the stability limit of phlogopite can form K-richterite in subduction zones. Mechanisms for the generation of K-enriched fluids from subducting slabs within the phlogopite stability field include: (1) breakdown of Ca-amphibole in the subducted slab (e.g. Tatsumi & Eggins, 1995); (2) decomposition of K-feldspar + phlogopite (Massonne, 1992); (3) continuous phengite dehydration or K-rich mid-ocean ridge basalt (MORB) melting (Schmidt, 1996; Domanik & Holloway, 1996); (4) hybridization between hydrous silicic melts and peridotitic mantle (Sekine & Wyllie, 1982; Wyllie & Sekine, 1982). Together, these mechanisms can form phlogopite in a large *P*(–*T*) interval within the mantle wedge. The presence of phlogopite in arc magma sources is supported by the occurrence of K-rich lamprophyric rocks in some young subduction zones (Esperança & Holloway, 1987; Hochstaedter *et al.*, 1996; Luhr, 1997). Moreover, some arc-related ophiolites contain phlogopite–calcic amphibole peridotites (Arai & Takahashi, 1990). Because phlogopite is stable to higher temperatures than is pargasite (see Wendlandt & Eggler, 1980; Mengel & Green, 1989), phlogopite can survive low-*P* partial melting of hydrated peridotite that extracts the Ca-amphibole. A possible source for K-rich fluids or hydrous melts at pressures exceeding the *P* stability of phlogopite is phengite breakdown to K-hollandite or melting of K-rich MORB, the latter occurring over a large *P* interval as a result of the low-angle intersection between typical subduction *P–T* paths and the solidus of K-rich MORBs (Domanik & Holloway, 1996; Schmidt, 1996; Sorensen *et al.*, 1997).

Fluid production during pressure-induced phlogopite breakdown

Tatsumi (1989), Tatsumi *et al.* (1991) and Tatsumi & Eggins (1995), on the basis of available experimental data (Sudo & Tatsumi, 1990), proposed that hydrous K-rich fluids are released during phlogopite breakdown to form potassium amphibole at a depth of ~180 km. These fluids are thought to trigger large-scale melting in the overlying mantle and be responsible for back-arc volcanism. Tatsumi & Eggins (1995) assumed that pure KK-richterite is formed from phlogopite breakdown, both phases having the maximum possible difference in their K/OH ratios. This assumption would yield the maximum amount of fluid that can be released during the phlogopite-to-amphibole reaction [reaction (2)]. A natural mantle environment that would approach the KCMASH system studied by Sudo & Tatsumi (1990) is a phlogopite–garnet peridotite, in which the grossular component of reactant garnet could provide Ca for the formation of KK-richterite (the diopside-absent reaction in Fig. 10b). In an Na-bearing system, the amount of fluid produced during phlogopite breakdown will be reduced because our experiments show that the first K-richterite stable in a subalkaline lherzolite composition contains significant amounts of Na and has a K/OH ratio very similar to that of phlogopite. Because nominally anhydrous minerals (NAMs) can accommodate significant amounts of water under high *P* and *T* conditions (e.g. Bell & Rossman, 1992; Young *et al.*, 1993; Kohlstedt *et al.*, 1996) it is uncertain whether small amounts of aqueous fluid can migrate through a mantle peridotite without being trapped by NAMs.

Experiments in the KNCMASH system indicate that phlogopite could persist to pressures as high as 8–9 GPa at 1100°C in peridotites with modal phlogopite > orthopyroxene, or in a relatively refractory peridotite bulk composition with very small amounts of Na-poor clinopyroxene. In such bulk compositions, phlogopite + K-richterite would coexist in a pressure interval of 2–3 GPa. In non-peridotitic, orthopyroxene-absent environments (phlogopite clinopyroxenites) the first K-richterite would form by clinopyroxene + phlogopite breakdown between 8 and 9 GPa.

Hydrous potassic phase composition from lherzolitic and MARID-type sources

Experimental K-richterite and phlogopite in equilibrium with a lherzolitic assemblage are similar in major element composition to their natural counterparts from metasomatized peridotites (PPs and PKPs; see Erlank *et al.*, 1987). This is not surprising, as PKP amphiboles have probably formed by metasomatic replacement of peridotite phases. Although experimentally grown K-richterite shows significantly higher Al contents at its lower *P* stability limit compared with PKP amphibole [see table I of Erlank *et al.* (1987)], this difference vanishes at very high pressures because of transfer of Al from phlogopite to garnet and clinopyroxene through Tschermak or combined Tschermak + plagioclase exchange. MARID-suite

K-richterite and phlogopite are higher in Fe and Ti compared with their peridotitic counterparts (Dawson & Smith, 1977; Erlank *et al.*, 1987; Waters, 1987*b*), which testifies to their origin from a different bulk composition. K-richterite and phlogopite from our experiments show Ni contents in the range of 640–1110 ppm and 1180–1730 ppm, respectively, values very similar to those reported for calcic amphibole and phlogopite in equilibrium with primary undifferentiated olivine (Griffin *et al.*, 1989) from various peridotitic mantle sources (Delaney *et al.*, 1980; O'Reilly *et al.*, 1991). For example, experimental K-richterite–olivine pairs from our experiments at 6·5 GPa and 1100°C and 8·0 GPa and 1100°C yield $D_{Ni}^{Kr/ol} = 0{\cdot}30 \pm 0{\cdot}08$ (six pairs) and $0{\cdot}31 \pm 0{\cdot}07$ (eight pairs), respectively. These values are identical to the $D_{Ni}^{Ca\text{-}amph/ol}$ of $0{\cdot}28 \pm 0{\cdot}04$ for coexisting pargasite and olivine from spinel peridotites reported by O'Reilly *et al.* (1991) in a T range between 825 and 1036°C, as well as to a value of 0·27 for the same partition coefficient determined by Mysen (1978) for coexisting pargasite + olivine + water-saturated liquid at 1·5 GPa and 1000°C. $D_{Ni}^{amph/ol}$ is insensitive to P and T (and amphibole composition) because Ni contents of peridotitic amphibole and phlogopite are buffered by coexisting olivine. On the other hand, MARID K-richterite and phlogopite are significantly lower in Ni, with values less than 570 and 860 ppm, respectively (Konzett, 1996) (Fig. 12). Assuming a $D_{Ni}^{Kr/ol}$ of 0·30, then olivine coexisting with MARID K-richterites must have had Ni contents of 1230–1440 ppm. This suggests that MARID amphibole and phlogopite did not crystallize in equilibrium with primary mantle olivine, but rather from a differentiated (presumably kimberlitic) melt that has undergone olivine fractionation with an attendant decrease of Ni.

ACKNOWLEDGEMENTS

We are indebted to Russell Sweeney and Alan Thompson for stimulating discussions. Sincere thanks are due also to Russell Sweeney for providing PIXE analyses of MARID phases. Careful and constructive reviews by George Harlow, Robert Luth and Gautam Sen are gratefully acknowledged. This study was financially supported by the Swiss National Science Foundation.

REFERENCES

Arai, S. & Takahashi, I. (1990). Formation and compositional variation of phlogopite in the Horoman peridotite complex, Hokkaido, northern Japan: implications for origin and fractionation of metasomatic fluids in the upper mantle. *Contributions to Mineralogy and Petrology* **101,** 165–175.

Bell, D. R. & Rossman, G. R. (1992). Water in Earth's mantle: the role of nominally anhydrous minerals. *Science* **255,** 1391–1397.

Brey, G. P. & Köhler, T. (1990). Geothermobarometry in four-phase lherzolites. Part II. New thermobarometers, and practical assessment of existing thermobarometers. *Journal of Petrology* **31,** 1353–1378.

Brey, G. P., Köhler, T. & Nickel, K. G. (1990). Geothermobarometry in four-phase lherzolites. Part I: Experimental results from 10 to 60 kb. *Journal of Petrology* **31,** 1313–1353.

Carpenter, M. A. & Smith, D. C. (1981). Solid solution and cation ordering limits in high temperature sodic pyroxenes from the Nybø eclogite pod, Norway. *Mineralogical Magazine* **44,** 37–44.

Davis, H. J. & Stevenson, D. J. (1992). Physical model of source region of subduction zone volcanics. *Journal of Geophysical Research* **97,** 2037–2070.

Dawson, J. B. & Smith, J. V. (1975). Occurrence of diamond in mica–garnet lherzolite xenolith from kimberlite. *Nature* **254,** 580–581.

Dawson, J. B. & Smith, J. V. (1977). The MARID (mica–amphibole–rutile–ilmenite–diopside) suite of xenoliths in kimberlite. *Geochimica et Cosmochimica Acta* **41,** 309–323.

Delaney, J. S., Smith, J. V., Carswell, D. A. & Dawson, J. B. (1980). Chemistry of micas from kimberlites and xenoliths: II Primary- and secondary-textured micas from peridotite xenoliths. *Geochimica et Cosmochimica Acta* **44,** 857–872.

Domanik, K. J. & Holloway, J. R. (1996). The stability and composition of phengitic muscovite and associated phases from 5·5 to 11 GPa: implications for deeply subducted sediments. *Geochimica et Cosmochimica Acta* **60,** 4133–4151.

Downes, H. (1987). Relationship between geochemistry and textural type in spinel lherzolites, Massif Central and Languedoc, France. In: Nixon, P. H. (ed.) *Mantle Xenoliths*. New York: John Wiley, pp. 125–133.

Droop, G. R. T., Lombardo, B. & Pognante, U. (1990). Formation and distribution of eclogite facies rocks in the Alps. In: Carswell, D. A. (ed.) *Eclogite Facies Rocks*. Glasgow: Blackie, pp. 225–256.

Erlank, A. J., Waters, F. G., Hawkesworth, S. E., Haggerty, H. L., Allsopp, R. S., Rickard, R. S. & Menzies, M. (1987). Evidence for mantle metasomatism in peridotite nodules from the Kimberley pipes, South Africa. In: Menzies, M. A. & Hawkesworth, M. C. (eds) *Mantle Metasomatism*. London: Academic Press, pp. 221–311.

Esperança, S. & Holloway, J. R. (1987). On the origin of some mica-lamprophyres: experimental evidence from a mafic minette. *Contributions to Mineralogy and Petrology* **95,** 207–216.

Finger, L. W. & Burt, D. M. (1972). REACTION, a FORTRAN IV computer program to balance chemical reactions. *Carnegie Institution of Washington, Yearbook* **71,** 616–620.

Foley, S. (1991). High-pressure stability of the fluor- and hydroxy-endmembers of pargasite and K-richterite. *Geochimica et Cosmochimica Acta* **55,** 2689–2694.

Foley, S. F. (1992). Vein-plus-wall-rock melting mechanisms in the lithosphere and the origin of potassic alkaline magmas. *Lithos* **28,** 435–453.

Furukawa, Y. (1993). Magmatic processes under arcs and formation of the volcanic front. *Journal of Geophysical Research* **98,** 8309–8319.

Griffin, W. L., Cousens, D. R., Ryan, C. G., Sie, S. H. & Suter, G. F. (1989). Ni in chrome pyrope garnets: a new geothermometer. *Contributions to Mineralogy and Petrology* **103,** 199–202.

Harlow, G. E. (1995). K-amphibole and mica stability in K-rich environments at high P and T. *EOS Transactions, American Geophysical Union* **76,** 298.

Hochstaedter, A. G., Ryan, J. G., Luhr, J. F. & Hasenaka, T. (1996). On B/Be ratios in the Mexican Volcanic Belt. *Geochimica et Cosmochimica Acta* **60,** 613–628.

Holland, T. J. B. (1988). Preliminary phase relations involving glaucophane and applications to high pressure petrology: new heat capacity and thermodynamic data. *Contributions to Mineralogy and Petrology* **99,** 134–142.

Kohlstedt, D. L., Keppler, H. & Rubie, D. C. (1996). Solubility of water in the α, β and γ phases of $(Mg, Fe)_2SiO_4$. *Contributions to Mineralogy and Petrology* **123,** 345–357.

Konzett, J. (1996). Phase relations and stability of potassium amphiboles in the Earth's mantle. An experimental investigation and a field-based study on MARID-type xenoliths. Ph.D. Thesis, Swiss Federal Institute of Technology, Zürich.

Konzett, J., Sweeney, R. J., Thompson, A. B. & Ulmer, P. (1997). Potassium amphibole stability in the upper mantle: an experimental study in a peralkaline KNCMASH system to 8·5 GPa. *Journal of Petrology* **38,** 537–568.

Kushiro, I. & Erlank, A. J. (1970). Stability of potassic richterite. *Carnegie Institution of Washington, Yearbook* **68,** 231–233.

Leake, B. E. (1978). Nomenclature of amphiboles. *American Mineralogist* **63,** 1023–1053.

Leake, B. E., Woolley, A. R., Arps, C. E. S., Birch, W. D., Gilbert, M. C., Grice, J. D., Hawthorne, F. C., Kato, A., Kisch, H. J., Krivovichev, V. G., Linthout, K., Laird, J., Mandarino, J. A., Maresch, W. V., Nickel, E. H., Rock, N. M. S., Schumacher, J. C., Smith, D. C., Stephenson, N. C. N., Ungaretti, L., Whittaker, E. J. W. & Youzhi, G. (1997). Nomenclature of amphiboles: report of the Subcommittee on Amphiboles of the International Mineralogical Association, Commission on New Minerals and Mineral Names. *American Mineralogist* **82,** 1019–1038.

Lloyd, F. E., Arima, M. & Edgar, A. D. (1985). Partial melting of a phlogopite–clinopyroxenite nodule from south-west Uganda: an experimental study bearing on the origin of highly potassic continental rift volcanics. *Contributions to Mineralogy and Petrology* **91,** 321–329.

Luhr, J. F. (1997). Extensional tectonics and the diverse primitive volcanic rocks in the western Mexican Volcanic Belt. *Canadian Mineralogist* **35,** 473–500.

Luth, R. W. (1997). Experimental study of the system phlogopite–diopside from 3·5 to 17 GPa. *American Mineralogist* **82,** 1198–1210.

Luth, R. W., Trønnes, R. G. & Canil, D. (1993). Volatile phases in the Earth's mantle. In: Luth, R. W. (ed.) *Experiments at High Pressure and Applications to the Earth's Mantle. Mineralogical Association of Canada Short Course Handbook* **21,** 445–485.

Maaløe, S. & Aoki, K-i. (1977). The major element composition of the upper mantle estimated from the composition of lherzolites. *Contributions to Mineralogy and Petrology* **63,** 161–173.

Massonne, H.-J. (1992). Evidence for low-temperature ultrapotassic siliceous fluids in subduction zone environments in the system K_2O–MgO–Al_2O_3–SiO_2–H_2O (KMASH). *Lithos* **28,** 421–435.

Mengel, K. & Green, D. H. (1989). Stability of amphibole and phlogopite in metasomatised peridotite under water-saturated and water-undersaturated conditions. In: Ross, J. (ed.) *Fourth International Kimberlite Conference. Australian Journal of Earth Sciences Special Publication* **14,** 571–581.

Mitchell, R. H. (1995). *Kimberlites, Orangeites and Related Rocks*. New York: Plenum, 410 pp.

Mysen, B. O. (1978). Experimental determination of nickel partition coefficients between liquid, pargasite, and garnet peridotite minerals and concentration limits of behaviour according to Henry's law at high temperatures and pressures. *American Journal of Science* **278,** 217–243.

Nixon, P. H. (ed.) (1987). *Mantle Xenoliths*. New York: John Wiley.

O'Reilly, S. Y., Griffin, W. L. & Ryan, C. G. (1991). Residence of trace elements in metasomatised spinel lherzolite xenoliths: a proton-microprobe study. *Contributions to Mineralogy and Petrology* **109,** 98–113.

Pollack, H. N. & Chapman, D. S. (1977). On the regional variation of heat flow, geotherms and lithospheric thickness. *Tectonophysics* **38,** 279–296.

Prider, R. T. (1939). Some minerals from the leucite-rich rocks of the West Kimberley area, Western Australia. *Mineralogical Magazine* **25,** 373–387.

Rossi, G. (1988). A review of the crystal-chemistry of clinopyroxenes in eclogites and other high-pressure rocks. In: Smith, D. C. (ed.) *Eclogites and Eclogite-Facies Rocks*. Amsterdam: Elsevier, pp. 237–270.

Schmidt, M. W. (1992). Phase compositions and relationships in tonalite: an experimental approach. Ph.D. thesis, Swiss Federal Institute of Technology, Zürich.

Schmidt, M. W. (1996). Experimental constraints on recycling of potassium from subducted oceanic crust. *Science* **272,** 1927–1930.

Seifert, F. & Schreyer, W. (1971). Synthesis and stability of micas in the system K_2O–MgO–SiO_2–H_2O and their relations to phlogopite. *Contributions to Mineralogy and Petrology* **30,** 196–215.

Sekine, T. & Wyllie, P. J. (1982). Phase relationship in the system $KAlSiO_4$–Mg_2SiO_4–SiO_2–H_2O as a model for hybridization between hydrous siliceous melts and peridotite. *Contributions to Mineralogy and Petrology* **79,** 368–374.

Smith, J. V., Delaney, J. S., Herwig, R. L. & Dawson, J. B. (1980). Storage of F and Cl in the upper mantle: geochemical implications. *Lithos* **14,** 133–147.

Sorensen, S. S., Grossman, J. N. & Perfit, M. R. (1997). Phengite-hosted LILE enrichment in eclogite and related rocks: implications for fluid-mediated mass transfer in subduction zones and arc magma genesis. *Journal of Petrology* **38,** 3–34.

Sudo, A. & Tatsumi, Y. (1990). Phlogopite and K-amphibole in the upper mantle: implications for magma genesis in subduction zones. *Geophysical Research Letters* **17,** 29–32.

Sweeney, R. J. (1994). Carbonatite melt compositions in the Earth's mantle. *Earth and Planetary Science Letters* **128,** 259–270.

Sweeney, R. J., Thompson, A. B. & Ulmer, P. (1993). Phase relations of a natural MARID composition and implications for MARID genesis, lithospheric melting and mantle metasomatism. *Contributions to Mineralogy and Petrology* **115,** 225–241.

Sweeney, R. J., Prozesky, V. & Przybylowicz, W. (1995). Selected trace and minor element partitioning between peridotite minerals and carbonatite melts at 18–46 kb pressure. *Geochimica et Cosmochimica Acta* **59,** 3671–3683.

Takahashi, E. (1986). Melting of a dry peridotite KLB-1 up to 14 GPa: implications on the origin of peridotitic upper mantle. *Journal of Geophysical Research* **91,** 9367–9382.

Tallarico, F. H. & Leonardos, O. H. (1995). Glimmeritic and peridotitic xenoliths from the Mata do Lenço micaceous kimberlite—Alto Paranaiba Igneous Province, Brazil: evidences of metasomatic processes in local mantle sources. *Sixth International Kimberlite Conference, Extended Abstracts*. Novosibirsk: United Institute of Geology, Geophysics and Mineralogy, Siberian Branch of Russian Academy of Sciences, pp. 600–602.

Tatsumi, Y. (1989). Migration of fluid phases and genesis of basalt magmas in subduction zones. *Journal of Geophysical Research* **94,** 4697–4707.

Tatsumi, Y. & Eggins, S. (1995). *Subduction Zone Magmatism*. Oxford: Blackwell Scientific.

Tatsumi, Y., Murasaki, M., Arsadi, E. M. & Nohda, S. (1991). Geochemistry of Quaternary lavas from NE Sulawesi: transfer of subduction components into the mantle wedge. *Contributions to Mineralogy and Petrology* **107,** 137–149.

Thibault, Y. (1993). The role of pressure and fluorine content in the distribution of K, Na, and Al in the upper mantle. *EOS Transactions, American Geophysical Union* **74,** 321.

Thibault, Y., Edgar, A. D. & Lloyd, F. E. (1992). Experimental investigation of melts from a carbonated phlogopite lherzolite: implications for metasomatism in the continental lithospheric mantle. *American Mineralogist* **77,** 784–794.

Thompson, A. B. (1983). Fluid-absent metamorphism. *Journal of the Geological Society, London* **140,** 533–547.

Thompson, A. B. (1992). Water in the Earth's upper mantle. *Nature* **358,** 295–302.

Thompson, J. B. (1982). Composition space: an algebraic and geometric approach. In: Ferry, J. M. (ed.) *Characterization of Metamorphism through Mineral Equilibria. Mineralogical Society of America, Reviews in Mineralogy* **10,** 1–32.

Trønnes, R. G. (1990). Low-Al, high-K amphiboles in subducted lithosphere from 200–400 km depth: experimental evidence. *EOS Transactions, American Geophysical Union* **71,** 1587.

Trønnes, R. G., Takahashi, E. & Scarfe, C. M. (1988). Stability of K-richterite and phlogopite to 14 GPa. *EOS Transactions, American Geophysical Union* **69,** 1510–1511.

Walker, D. (1991). Lubrication, gasketing, and precision in multianvil experiments. *American Mineralogist* **76,** 1092–1100.

Walker, D., Carpenter, M. A. & Hitch, C. M. (1990). Some simplifications to multianvil devices for high pressure experiments. *American Mineralogist* **75,** 1020–1028.

Waters, F. G. (1987*a*). A suggested origin of MARID xenoliths in kimberlites by high pressure crystallization of an ultrapotassic rock such as lamproite. *Contributions to Mineralogy and Petrology* **95,** 523–533.

Waters, F. G. (1987*b*). A geochemical study of metasomatised peridotite and MARID nodules from the Kimberley pipes, South Africa. Ph.D. Thesis, University of Cape Town.

Waters, F. G. & Erlank, A. J. (1988). Assessment of the vertical extent and distribution of mantle metasomatism below Kimberley, South Africa. *Journal of Petrology, Special Lithosphere Issue* 185–204.

Wendlandt, R. F. & Eggler, D. H. (1980). The origins of potassic magmas: 2. Stability of phlogopite in natural spinel lherzolite and in the system $KAlSiO_4$–MgO–SiO_2–H_2O–CO_2 at high pressures and high temperatures. *American Journal of Science* **280,** 421–458.

Wyllie, P. J. & Sekine, T. (1982). The formation of mantle phlogopite in subduction zone hybridization. *Contributions to Mineralogy and Petrology* **79,** 375–380.

Young, T. E., Green, H. W., Hofmeiser, A. M. & Walker, D. (1993). Infrared spectroscopic investigation of hydroxyl in beta-Mg_2SiO_4 and coexisting olivine; implications for mantle evolution and dynamics. *Physics and Chemistry of Minerals* **19,** 409–422.